

Plant-Denoising-Net (PDN): A plant point cloud denoising network based on density gradient field learning

Jianeng Wu ^a, Lirong Xiang ^b, Hui You ^{a,c}, Lie Tang ^d, Jingyao Gai ^{a,*}

^a School of Mechanical Engineering, Guangxi University, Nanning, Guangxi 530004, China

^b Department of Biological & Agricultural Engineering, North Carolina State University, Raleigh, NC 27695, USA

^c Guangxi Key Lab of Manufacturing System and Advanced Manufacturing Technology, Nanning, Guangxi 530004, China

^d Department of Agricultural and Biosystems Engineering, Iowa State University, Ames, IA 50011-3270, USA



ARTICLE INFO

Keywords:

Point cloud denoising
Deep learning
Phenotyping
Multi-feature fusion
Density gradient field
Gradient ascent

ABSTRACT

Effective point cloud denoising is critical in 3D plant phenotyping applications, which reduces interference in subsequent algorithms and improves the accuracy of plant phenotypes measurement. Deep learning-based point cloud denoising algorithms have shown excellent denoising performance on simple CAD models. However, these algorithms suffer from issues including over-smoothing or shrinkage and low efficiency when applied on density uneven, incomplete, various types of noise and complex plant point clouds. We proposed a plant point cloud denoising network (PDN) based on point cloud density gradient field learning, which can effectively address the challenges posed by plant point clouds. PDN consists of three main modules: point density feature (PDF) exception module, umbrella operator feature (UOF) computation module, and point density gradient (DG) estimation module. The performance of PDN was evaluated in experiments using point clouds of multiple plant species with noise of different types. Under different levels of Gaussian noise, our method achieved a relative performance improvement of 7.6%–19.3% compared to the state-of-the-art baseline methods, reaching state-of-the-art denoising performance. For noise of different types, the majority of our denoising results outperformed the baseline methods. In addition, our method was 0.5 and 8.6 times faster than the baseline methods when processing point clouds with low and high noise level, respectively. The good robustness, generalization, and computational efficacy of PDN are expected to facilitate the acquisition of high-precision 3D point clouds for various plant species, enhance the versatility of 3D phenotyping methods, improve the accuracy of the measurement of structural phenotypes, and increase the throughput of data processing, therefore facilitate the development of modern breeding research. The source code and the datasets used in this study is available on GitHub at <https://github.com/suetme/PDN-plant-denoising-net>.

1. Introduction

Ensuring a sustained supply of food and feed, addressing resource shortages, mitigating the impacts of climate change, and managing energy consumption are significant challenges we face in our dependence on plant resources (Zhao et al., 2019). Plant phenotyping is an emerging technology to bridge the gap between genomics, plant function and agricultural traits (Fan et al., 2021). Plant structural phenotype, which refers to the morphological traits of plant organs, such as leaf area and stem length (Das Choudhury et al., 2019), plays an crucial role in applications like crop breeding and growth monitoring. Traditional methods for obtaining plant structural phenotypes mainly rely on

manual measurements using handheld measuring devices, which are subjective, labor intensive, less efficient, and may cause plant damage (Du et al., 2023). These issues limit the throughput and precision of the collection of plant structural phenotype for the subsequent GWAS studies, which becomes a bottleneck for the development of modern breeding research (White et al., 2012). The advent of computer vision techniques has revolutionized the quantification of plant structural phenotypes, offering non-invasive, high-precision and automatic solution (Li et al., 2020).

While 2D image-based phenotyping approaches often acquire images from a single perspective, limiting their ability to analyze the structure of the entire plants and suffering from frequent occlusions (Li et al.,

* Corresponding author.

E-mail address: jygai@gxu.edu.cn (J. Gai).

2022), the introduction of 3D measurement techniques in plant phenotyping has addressed these limitations (Turgut et al., 2022b). Leveraging 3D sensors, these methods utilize spatial information to achieve higher precision in the measurements of plant structural phenotypes, acquiring data in the format of 3D point clouds (Paturkar et al., 2021).

However, due to hardware errors of the 3D sensors and environmental interference, the collected point cloud data is inevitably perturbed by noise, including outliers, uneven density, and incompleteness (Wu et al., 2018). Point clouds with noise will significantly impact the performance of point cloud processing algorithms, such as registration (Zhu et al., 2023b), segmentation (Boogaard et al., 2022; Turgut et al., 2022a), surface reconstruction (Boukhana et al., 2022), and cylinder fitting (Lin et al., 2022), leading to decreased performance in extracting plant structural phenotypes (Ghahremani et al., 2021). Therefore, point cloud denoising is a critical step in plant 3D phenotypic measurement methods. Nevertheless, the complex structure, uneven density, incompleteness, and the diverse types of noise and species make denoising of plant point clouds a challenging task.

Among the traditional point cloud denoising approaches used in plant 3D phenotyping methods, the most widely used algorithms are Statistical Outlier Removal (SOR) (Ao et al., 2022; Gu et al., 2022; Liu et al., 2023; Wei et al., 2023), radius filtering (Song et al., 2023; Wu et al., 2019), and DBSCAN (Zermas et al., 2020). However, these general-purpose denoising algorithms can only remove obvious outliers from dense point clouds and worsen the challenges of the uneven density and incompleteness within the point cloud itself (Li et al., 2023), thus less effectively for point clouds collected by 3D sensors with limited precision. For plant phenotyping applications focusing on the leaf traits such as leaf area and leaf shape, researchers used Moving Least Squares (MLS) for surface smoothing (Boukhana et al., 2022; Chaiyivatrakul et al., 2014; Yamamoto et al., 2018; Yau et al., 2021). While this technique contributes to a partial reduction of noise in point clouds, it tends to cause over-smoothing unless carefully tuned according to the plant species, making it challenging to preserve the fine details of plants (Zhang et al., 2021). Additionally, some methods are only effective for specific plant species (Lu et al., 2020) or exhibit low denoising efficiency (Zhu et al., 2023a). Generally, traditional point cloud denoising methods were selected or designed for specific applications, according to plant species, data quality and noise types, relying heavily on geometric priors (Chen et al., 2022). Moreover, parameter tuning processes are necessary for most traditional methods to achieve faster convergence rate and better visual quality of denoising (Li et al., 2023).

Recently, the emergence of point feature extraction networks (Qi et al., 2017a; Wang et al., 2019) has facilitated the realization of point cloud denoising with deep learning. Denoising methods based on deep learning (Rakotosaona et al., 2020; Luo & Hu, 2020; Luo & Hu, 2021; Wang et al., 2023) demonstrate superior performance compared to many traditional approaches. However, these approaches demonstrate sensitivity to point cloud density (Huang et al., 2022), revealing limitations in addressing the uneven density of plant point clouds. Their constrained generalizability (Li et al., 2023) hinders adaptation to diverse plant species and noise types, and their iterative nature (Zhao et al., 2023) becomes impractical when confronted with the substantial volume of plant point cloud data. Though advanced denoising performance has been reported, the tangible contributions of these methods in the research community remains unclear, as experiments often conducted on point clouds uniformly sampled on relatively simple CAD models (Choi et al., 2022). To enable a robust assessment and comparison of plant point cloud denoising methods, there is an urgent need for an open-access benchmark dataset with diverse plant species and noise types. Unfortunately, such a dataset is lacking.

To summarize, the challenges of currently available denoising methods in 3D phenotyping applications were mainly imposed by:

1. The unevenness in density and the potential incompleteness of the collected plant point clouds;
2. The lack of assumptions of noise type in collected point clouds due to the variations in agricultural environments and sensor specifications;
3. The diversity of plant species studied in phenotyping applications, thus requiring development of species-specific geometric priors for prior-based denoising methods;
4. The demand of high throughput to process massive amount of plant point clouds in phenotyping tasks to accelerate modern crop breeding research;
5. The lack of an open-access benchmark dataset with diverse plant species and noise types to evaluate and compare deep learning-based methods.

This paper proposed an plant point cloud denoising method based on density gradient field learning. Unlike conventional methods, This technique does not depend on geometric priors and extensive iterations. Consequently, it adeptly addresses the challenges associated with denoising plant point clouds. Additionally, an open-access dataset has been created for evaluating and comparing the denoising performance of plant point clouds using deep learning-based methods.

2. Related work

In this section, we primarily review point cloud denoising methods based on deep learning that are most relevant to our work. The advent of 3D point feature extraction networks based on deep learning, represented by PointNet (Qi et al., 2017a), PointNet++ (Qi et al., 2017b) and DGCNN (Wang et al., 2019), has facilitated the development of point cloud denoising based on deep learning. Reported denoising methods based on deep learning can be broadly characterized as: displacement-prediction-based (Chen et al., 2022; Pistilli et al., 2020; Rakotosaona et al., 2020), resampling-based (Xu et al., 2022; Casajus et al., 2019; Luo & Hu, 2020) and probability-density-based (Zhao et al., 2023; Wang et al., 2023; Luo & Hu, 2021).

Focusing initially on displacement-prediction-based methods, these approaches extract features of the noisy points using a point feature extraction network and predict displacement for each point to recover a noise-free point cloud. For instance, Point Clean Net (PCN) (Rakotosaona et al., 2020) utilizes a variant of PointNet, named PCPNet (Guerrero et al., 2018), to predict the offset of each point from the potential surface. RePCD-Net (Chen et al., 2022) adopts a recurrent neural network architecture to address the issue of feature variations not being captured in the iterative denoising process of PCN. However, these methods sensitive to point cloud density, noise levels, and geometric shape variations (Huang et al., 2022). Additionally, the extensive network parameters and iterative denoising approach result in inefficient denoising (Li & Sheng, 2023). Such limitations make these methods unsuitable for handling the uneven density of plant point clouds and the need for substantial data throughput.

Transitioning to resampling-based methods, these techniques extract points features using a neural network and sample low-noise points based on these features. Then, the sampled points are used to reconstruct the underlying surface of the noisy point cloud. Finally, resampling is performed on the reconstructed surface to recover the denoised point cloud. The key to these methods is to filter out low-noise points from the noisy point cloud. For example, Differentiable Manifold Reconstruction (DMR) (Luo & Hu, 2020) used differentiable pooling filter out low-noise points. In contrast, TDNet (Xu et al., 2022) achieves a more robust filtering of low-noise points through the use of an adaptive sampling module. These methods avoid iteration by utilizing resampling, and the robust fitting capability of neural networks allows for easy decoding of the latent surface from point cloud features, leading to a significant reduction in network parameters. However, These methods show limited generalization, struggling to adapt to the diversity of plant species, as they tend to learn the underlying geometric representations

of the training data, incorporating certain geometric priors (Li et al., 2023).

On the contrary, probability-density-based methods exhibit better generalization. These methods treat noisy point cloud as a distribution and model the gradient of the logarithmic probability density function of this distribution using a neural network. Gradient ascent is then performed on this gradient with respect to the noisy point cloud to obtain the denoised point cloud. For instance, Score-based Denoising (SD) (Luo & Hu, 2021) is a deep neural network that performs point cloud denoising in this manner and has achieved state-of-the-art performance in point cloud denoising. Wang et al. (2023) incorporated a hybrid attention mechanism into the feature extraction module of SD to amplify information from relevant points and suppress that from outliers. However, inaccurate density gradient estimates from such methods exacerbate uneven density and incompleteness in point clouds (Zhao et al., 2022). Multiple iterations may be needed for noisy point clouds for better denoising quality, with the cost of efficiency (Zhao et al., 2023).

Inspired by PointSIFT (Jiang et al., 2018), incorporating some directional information into neural networks can effectively reduce sensitivity to point cloud density and scale variations. The proposed method enhances the accuracy of density gradient estimation by fusing a umbrella operator (Desbrun et al., 1999) whose direction highly correlated with density gradient, thus eliminating the need for excessive iterations. Although deep learning-based point cloud denoising methods have been tested on point clouds uniform sample on relatively simple CAD models (Choi et al., 2022), their performance on the collected point clouds of plants was seldomly studied. Therefore, we have created an open-access plant point cloud benchmark dataset with diverse plant species and noise types for evaluating and comparing the denoising performance of deep learning-based methods. The contributions of this paper are summarized as follows:

1. We proposed a novel denoising network based on density gradient field learning in order to overcome the major challenges of uneven density and incompleteness.
2. We employ a density-gradient-based point cloud denoising approach that is independent of geometric priors, noise types and plant species, showcasing strong generalizability and robustness.
3. We encode point density features to accurately estimate density gradients by utilizing a multi-feature fusion approach. This enables us to achieve state-of-the-art denoising performance and eliminates the need for iterative gradient ascent during the denoising process, thus satisfying high-throughput requirements.
4. We constructed a dataset of noisy point clouds of plants of various species, with various levels and various types of noise. This dataset could be a valuable source for investigating the generalizability of denoising algorithms.

3. Methods

3.1. Denoising theory

A point cloud can be viewed as a set of points sampled from the surface of a 3D object. A surface can be modeled as a distribution $Q(\mathbf{x})$ supported by a 2D manifold. The probability density function is $q(\mathbf{x})$, $\mathbf{x} \subseteq \mathbb{R}^3$. From distribution $Q(\mathbf{x})$, it is possible to randomly sample a noise-free point cloud $X = \{\mathbf{x}_i\}_{i=1}^n$ to represent the surface. The noise vector of each point can be modeled as a distribution $N(\mathbf{x})$ with a probability density function $n(\mathbf{x})$. Therefore, a noisy point cloud can be modeled as a set denoted as $Y = \{\mathbf{y}_i = \mathbf{x}_i + \boldsymbol{\epsilon}_i\}_{i=1}^n$, in which $\boldsymbol{\epsilon}_i \sim N(\mathbf{x})$ is a noise vector for each point. As the probability density function of the sum of two independent random variables, the probability density function $d(\mathbf{x})$ of distribution $D(\mathbf{x})$, from which the noisy point cloud was sampled, is:

$$d(\mathbf{x}) = (q * n)(\mathbf{x}) = \int_{s \in \mathbb{R}^3} q(s)n(\mathbf{x} - s)ds, \quad (1)$$

The objective of denoising is to come up with an parametrized approximate distribution $\hat{Q}(\mathbf{x}; \hat{\boldsymbol{\alpha}})$ for the distribution $Q(\mathbf{x})$, from which a noise-free point cloud can be sampled. $\hat{Q}(\mathbf{x}; \hat{\boldsymbol{\alpha}})$ can be solved by integrating the approximate parameterize probability density function $q(\mathbf{x}; \hat{\boldsymbol{\alpha}})$ for $q(\mathbf{x})$:

$$\hat{Q}(\mathbf{x}; \hat{\boldsymbol{\alpha}}) = \int_{\mathbf{x} \in \mathbb{R}^3} q(\mathbf{x}; \hat{\boldsymbol{\alpha}})d\mathbf{x}, \quad (2)$$

Ideally, by assuming that the noise $N(\mathbf{x})$ follows a certain distribution, and $d(\mathbf{x})$ is estimated by using the noisy point cloud Y , $q(\mathbf{x}; \hat{\boldsymbol{\alpha}})$ can be calculated by taking the derivative of the both sides of equation (1). However, the distribution of the noise collected from a 3D sensor is typically an unknown non-normalized distribution, and it is numerically inapplicable to estimate an parametrized distribution of $d(\mathbf{x})$ through maximum likelihood estimation (MLE) from the noisy data directly.

In order to address the challenge of estimating $d(\mathbf{x})$ from noisy data, Luo & Hu (2021) proved that denoising a noisy point cloud is equivalent to select a set of points $\hat{X} = \{\hat{\mathbf{x}}_i\}_{i=1}^n$ to maximize the joint probability $\prod_{i=1}^n d(\mathbf{x}_i)$, which is $\sum_{i=1}^n \log d(\mathbf{x}_i)$ in its logarithm form. Therefore, gradient ascent technique can be performed using the gradient of log-probability density function $\nabla_{\mathbf{x}} \log d(\mathbf{x})$ in order to denoise. The log-probability density function $\nabla_{\mathbf{x}} \log d(\mathbf{x})$ is estimated using score matching technique (Hyvärinen, 2005), in which a parameterized score function model $\mathcal{S}(\mathbf{x}; \xi)$ was fitted to minimize the distance between the model-predicted score and the actual score $s(\mathbf{x}) = \nabla_{\mathbf{x}} \log d(\mathbf{x})$. The objective function for score matching is:

$$\mathcal{J}(\xi) = \mathbb{E}[\|s(\mathbf{x}) - \mathcal{S}(\mathbf{x}; \xi)\|_2^2], \quad (3)$$

$$\xi^* = \operatorname{argmin}_{\xi} \mathcal{J}(\xi), \quad (4)$$

And the process of performing gradient ascent on the noisy point cloud is equivalent to maximizing the following objective function:

$$\hat{X} = \{\hat{\mathbf{x}}_i\}_{i=1}^n = \operatorname{argmax}_{\mathbf{x}_i} \sum_{i=1}^n \log d(\mathbf{x}_i; \xi), \quad (5)$$

From the two objective functions (equation (4) and (5)) mentioned above, it can be inferred that the point cloud denoising process based on gradient ascent is an end-to-end process. Therefore, we propose PDN, an end-to-end neural network, to learning the gradient field $\nabla_{\mathbf{x}} \log d(\mathbf{x})$ that can accurately estimate the gradient of each point, then perform gradient ascent (Fig. 1), achieving more advanced denoising performance. In summary, the denoising approach based on density gradient prediction is independent of any geometric priors, noise distributions and plant species, and can robustly handle various challenges posed by plant point clouds.

3.2. Plant denoising network architecture

PDN is a network proposed for denoising plant point clouds based on point density gradient prediction and gradient ascent (Fig. 2), which mainly includes three modules: point density feature (PDF) extraction module, umbrella operator feature (UOF) calculation module, and point density gradient (DG) estimation module. PDF extraction module extracts local features of points and maps them to higher-order point density features. This feature effectively addresses the challenges of uneven density and incompleteness of plant point cloud. UOF calculation module calculates the local umbrella operators of points as the umbrella operator features. This feature serves as a boundary condition for predicting the point density gradient to avoid severe deviations and mitigates the issue of hole expansion caused by incompleteness of plant

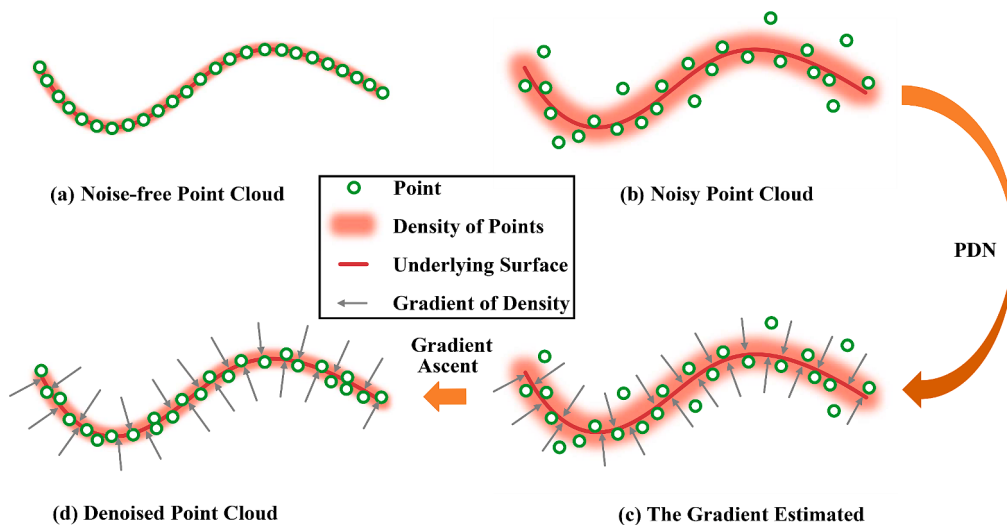


Fig. 1. Overview of the proposed method. (a) is the noise-free point cloud. (b) is the point cloud disturbed by noise. (c) is the gradient estimated by PDN. (d) is the denoised point cloud obtained by performing gradient ascent along the direction of the gradient with noisy point cloud.

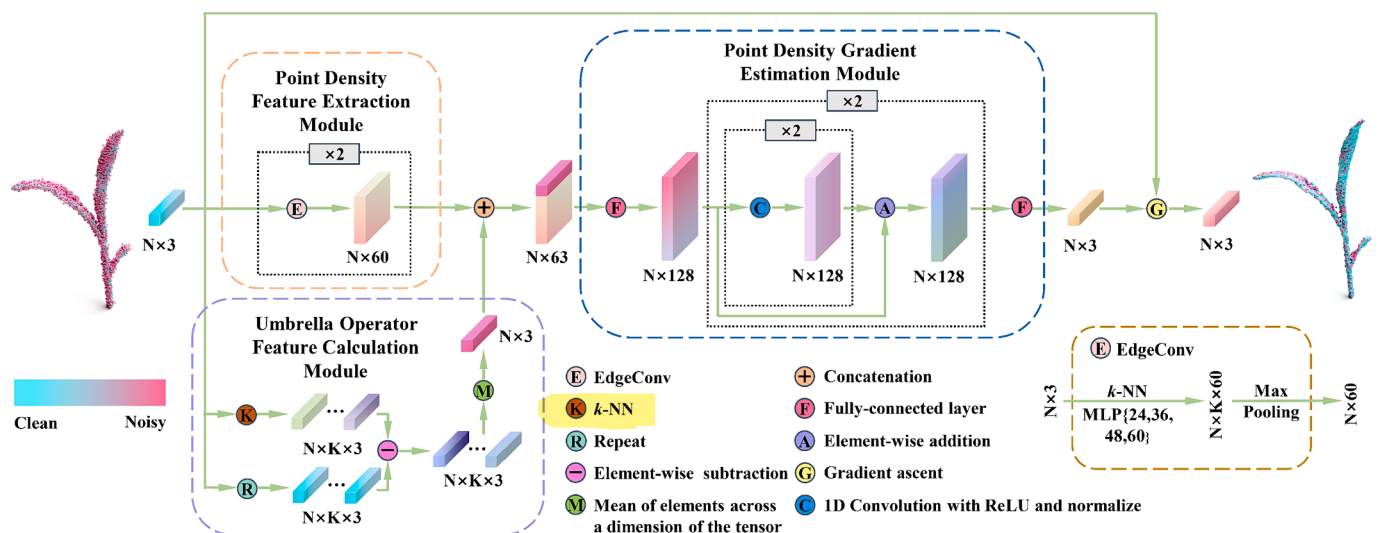


Fig. 2. The overall framework of PDN.

point cloud during gradient ascent. DG estimation module applies to the fused features of the UOF and PDF. Finally, gradient ascent is performed on the predicted DG to achieve denoising.

3.2.1. Point density feature (PDF) extraction module

The key to the denoising method based on density gradients is the ability to effectively extract point density features to address the challenges of uneven density and incompleteness of plant point cloud. The point density is a feature related to the spatial distribution of the points around a certain point, and the feature is critical in the estimation of point density gradient. In our PDN, a PDF extraction module was proposed to extract PDF of a point in the cloud by constructing the local spatial features of points. Edge convolution (EdgeConv) (Wang et al., 2019) was used to construct the PDF extraction module. EdgeConv module encodes the local neighbors of a point in manner of directed graph, then abstracts the point and adjacent edges as edge feature vectors using MLP, and finally aggregates the edge feature vectors into the local spatial feature of the point using max-pooling (Fig. 3). The detailed mechanics is stated as follows:

Consider a set of n feature points in F -dimensional feature space, denoted as $\mathcal{P} = \{p_1, \dots, p_n\} \subseteq \mathbb{R}^F$. For each feature point p_i in the points

set P , EdgeConv firstly constructs a directed graph $\mathcal{G} = (\mathcal{V}, \mathcal{E})$ (Fig. 3) of the point to represent the local neighbors of the point in the F -dimensional space by using k -NN algorithm (Keller et al., 1985). Here, $\mathcal{V} = \{j_1, \dots, j_k\}$ and $\mathcal{E} \subseteq \mathcal{V} \times \mathcal{V}$ are the vertices and edges of the directed graph, respectively. The edge feature $e_{ijm} \subseteq \mathbb{R}^F$ (Fig. 3) is defined as:

$$e_{ijm} = \left\{ h_\Theta(p_i, p_{jm} - p_i) \right\}_{m=1 \dots k}, \quad (6)$$

where h_{Θ} defines a mapping of $\mathbb{R}^F \times \mathbb{R}^F \rightarrow \mathbb{R}^F$ operated by a shared parameter multi-layer perceptron (MLP) with a learnable parameter set Θ . Then, a max-pooling operation which aggregates the edge features was used to extract the local spatial feature $p_i \subseteq \mathbb{R}^F$ (Fig. 3) of the point:

$$p_i = \max_{m=1 \dots k} e_{ijm}, \quad (7)$$

In order to abstract the local spatial feature of a point into higher-order point density features, two EdgeConv modules were concatenated in PDN to construct the point density feature extraction module. Each EdgeConv module used a four-hidden-layers MLP with 24, 36, 48, and

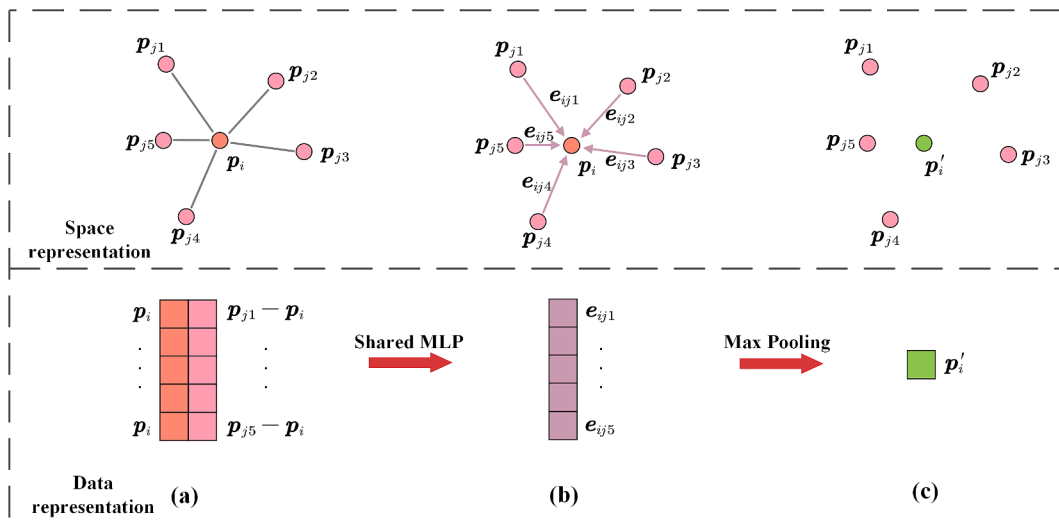


Fig. 3. Illustration of EdgeConv. (a) is the directed graph of p_i . (b) is edge feature. (c) is local feature p'_i .

60 neurons in each hidden layer, respectively.

3.2.2. Umbrella operator feature (UOF) calculation module

Accurate density gradient enable the noisy point clouds to move in the correct direction, thereby alleviating the challenge of holes expansion caused by incompleteness of plant point cloud during gradient ascent. An umbrella operator (Desbrun et al., 1999) feature calculation module was adopted in the proposed PDN network aimed to improve the performance of gradient estimation. It calculates the UOF of each point as follows:

For each point p_i in the point cloud P , k -NN algorithm was applied to find k -nearest points and calculates a vector $\mathbf{n}_{il} \subseteq \mathbb{R}^3$ joining p_i to each of the k points, then the UOF of point p_i was calculated as the average of these displacement vectors:

$$\mathbf{n}_i = \frac{1}{k} \sum_{l=1}^k \mathbf{n}_{il} = \frac{1}{k} \sum_{l=1}^k (\mathbf{p}_l - \mathbf{p}_i). \quad (8)$$

As observed, the umbrella operator feature is always correlated with the point density gradient (Fig. 4). Therefore, the proposed PDN network can learn from this correlation to improve the accuracy of point density gradient estimation. The UOF provides a boundary condition for the PDN network to solve the point density gradient, which ensures that the direction of movement of noise points does not deviate significantly from the correct direction and result in outliers or holes expansion.

3.2.3. Point density gradient (DG) estimation module

In order to enhance the accuracy of estimated point density gradient, iterative optimization of density gradient is commonly employed, which results in inefficient processing of the algorithm. Utilizing multi-feature fusion allows for obtaining more robust features, thereby improving the accuracy of point density gradients, reducing the number of iterations,

and meeting the high-throughput requirements of 3D plant phenotyping. The DG estimation module was designed to fuse the calculated PDF and UOF, then estimate the point density gradient. The details are as follows:

First, a fully connected layer was used to fuse the PDF (p'_i) and the UOF (n_i) into a fused feature $f_i \subseteq \mathbb{R}^S$:

$$f_i = FC[Cat(p'_i, n_i)], \quad (9)$$

where $Cat(\bullet, \bullet)$ represents a concatenation operation of two tensors, and $FC(\bullet)$ represents a fully connected layer.

Then, an implicit expression g_i of the point DG was calculated for each fused feature f_i , which can be formulated as:

$$g_i = Grad_{\Psi}(f_i), \quad (10)$$

where $Grad_{\Psi}(\bullet) : \mathbb{R}^S \rightarrow \mathbb{R}^S$ represents a MLP network with a learnable parameter set Ψ . The MLP was designed as two residual blocks, which can effectively reduce feature loss and alleviate the problem of gradient vanishing (He et al., 2016). Each block consisted of two hidden layers, and the number of neurons in each hidden layer was 128.

Meanwhile, a fully connected layer was used to map the implicit expression of point DG g_i in the fusion feature space \mathbb{R}^S to the point density gradient in the three-dimensional space \mathbb{R}^3 , denoted as $\hat{s}_i \subseteq \mathbb{R}^3$:

$$\hat{s}_i = FC(g_i), \quad (11)$$

Finally, by performing gradient ascent along the estimated point density gradient direction, we can obtain the denoised point \hat{p}_i :

$$\hat{p}_i = p_i + \alpha \hat{s}_i, \quad (12)$$

where α is the step size of gradient ascent and was set to 1 in this study. Depending on the noise level of the point cloud, multiple iterations may be needed until best denoising performance were obtained.

3.3. Loss function

As described in section 3.1, the clean (noise-free) point cloud was defined as $X = \{x_i\}_{i=1}^n$ and the noisy point cloud was defined as $Y = \{y_i\}_{i=1}^n$. As shown in the network structure in section 3.2, the final prediction of PDN is the density gradient \hat{s}_i of the noisy point, which points to the region of maximum density in the noisy point cloud, indicating the location of the underlying surface. Therefore, to define the network loss, we first defined the true density gradient s_i from the

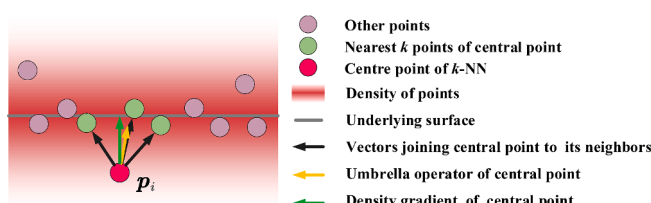


Fig. 4. Illustration of the correlation between umbrella operator and density gradient.

noisy point to the underlying surface. Let $X_{ki} = \{x_{il}\}_{l=1}^k$ be the set of the k -nearest points in X to y_i . Then, s_i was defined as:

$$s_i = \frac{1}{k} \sum_{l=1}^k (x_{il} - y_i), \quad (13)$$

Since the network estimates gradient in Euclidean space, we used L2 norm to calculate the gradient loss. The loss function of PDN was defined as:

$$\mathcal{L} = \frac{1}{n} \sum_{i=1}^n \|\hat{s}_i - s_i\|_2^2. \quad (14)$$

4. Experiments

4.1. Dataset preparation

To comprehensively evaluate the performance of our proposed plant point cloud denoising network (PDN), we conducted a series of experiments designed to quantitatively assess its effectiveness in various aspects. To this end, we created a diverse set of datasets, each with distinct characteristics and corresponding ground truth, to evaluate the versatility of our PDN approach in different scenarios.

Dataset A was created for training the proposed denoising network, as well as to evaluate the denoising performance on different types of noise, including Gaussian noise, Laplace noise, uniform noise and discrete noise. We selected 90 high quality 3D point clouds of maize plants from the dataset shared by Miao et al. (2021) and the Phne04D dataset shared by Schunck et al. (2021). These point cloud datasets cover the V2-V8 growth stages of the maize and were created using high accuracy laser scanners.

Dataset B was created to validate the generalizability of the proposed network to different plant species. 10 point clouds of other plants (e.g. Arabidopsis, tomato, and sorghum) from the Phne04D dataset and the 3D plant dataset released by Conn et al. (2017) were selected for denoising performance testing.

Dataset C was created to validate the effectiveness of the proposed method in mitigating the issues of uneven density and incompleteness inherent in plant point clouds. We selected 10 maize point clouds from Phne04D, and downsampled the point clouds at varying rates across different regions, thereby emulating the uneven density effect typically observed in data collected via vision sensors. We also removed certain regions within the clouds to simulate occlusion during data acquisition, resulting in incompleteness in point clouds. The processing of these point clouds was performed manually utilizing the open-source tool, CloudCompare.

Dataset D was created to assess the versatility of the proposed method when applied to point clouds of plant organs exhibiting a variety of geometric forms, including stems with cylindrical features, and leaves with slice features. We manually segment plant point clouds derived from the previously mentioned three open-source datasets using CloudCompare, which contains 8 leaf from maize, Arabidopsis, tomato, and tobacco point clouds, and 8 stem from maize point clouds.

The outliers, ground points, and excessive redundant points in these point clouds were manually removed using CloudCompare. The spatial resolution of points were controlled to be consistent with the field and indoor-collected data (Xiang et al., 2021) in high-throughput phenotyping applications using voxel downsampling algorithm in PCL (Rusu & Cousins, 2011), which reduced the size of point clouds to 5 K-20 K. After these processing steps, clean point clouds were obtained. Then the scales of these noise-free point clouds were normalized to fit within a unit sphere for consistency. The normalization process can be formulated as follows:

Let $X = \{x_i = (u_i, v_i, w_i)\}_{i=1}^n$ be the clean point cloud, where X has maximum values of U_{max} , V_{max} , and W_{max} , and minimum values of U_{min} , V_{min} , and W_{min} along the three coordinate axes, respectively. The

center of the point cloud is:

$$\mathbf{x}_c = (u_c, v_c, w_c) = \frac{1}{2}(U_{max} + U_{min}, V_{max} + V_{min}, W_{max} + W_{min}), \quad (15)$$

The transformation scale factor t for scaling to a unit sphere is:

$$t = \max_{i=1,\dots,n} \sqrt{(u_i - u_c)^2 + (v_i - v_c)^2 + (w_i - w_c)^2}, \quad (16)$$

The normalized result of the clean point cloud \bar{X} is therefore:

$$\bar{X} = \frac{1}{t} \{\bar{x}_i = \mathbf{x}_i - \mathbf{x}_c\}_{i=1}^n. \quad (17)$$

For the purpose of network training, 75 point clouds of maize plants were randomly extracted from Dataset A. The testing datasets, on the other hand, were composed of a diverse selection of point clouds to evaluate the network's denoising performance from various perspectives (Table 1). This included 15 point clouds of maize plants, 10 point clouds of other plant species, 10 point clouds of maize plants exhibiting uneven density and incompleteness, along with 8 point clouds each of leaves and stems.

For the point clouds in the training dataset, Gaussian noise was introduced to the normalized noise-free point clouds \bar{X} using the following Gaussian noise model:

$$G(\bar{X}, s) = \frac{1}{\sqrt{2\pi}s} e^{-\frac{|\bar{X}|^2}{2s^2}}, \quad (18)$$

where s is the noise level parameter. For each training point cloud, we randomly set s to a value between 0.5 % and 1 % of the unit sphere radius to obtain different levels of noise. Since the number of points in the training point cloud varies, and the neural network can only accept input of a fixed number of points, the farthest point sampling algorithm (Qi et al., 2017b) and k -nearest neighbor algorithm were applied to divide a point cloud into multiple point clouds blocks with a point number of 1 K before training the network.

For the point clouds in the testing dataset, we used the Gaussian noise model to perturb the testing point clouds, the noise level s was set to 0.5 %, 1 %, 1.5 %, and 2 % of the radius of the unit sphere. In order to evaluate the denoising performance to noise types other than Gaussian noise, we performed tests on point clouds with various types of noise, including Laplacian noise, uniform noise, and discrete noise. For Laplacian noise, we used the following model to perturb the testing point clouds:

$$L(\bar{X}, s) = \frac{1}{2s} e^{-\frac{|\bar{X}|}{s}}, \quad (19)$$

As with the Gaussian noise model, s is the noise level parameter, which is set to 0.5 %, 1 %, 1.5 %, and 2 % of the radius of the unit sphere. For uniform noise, we used the following model to perturb the testing point clouds:

$$U(\bar{X}, s) = \begin{cases} \frac{3}{4\pi s^3} & \|\bar{X}\|_2 \leq s \\ 0 & \text{Otherwise} \end{cases}. \quad (20)$$

For discrete noise, we used the following model to perturb the testing

Table 1

The distribution of the point clouds used for training and testing.

Dataset	Point cloud type	Train	Test	Total
Dataset A	Maize	75	15	90
Dataset B	Other Species	0	10	10
Dataset C	Maize (uneven density and incompleteness)	0	10	10
Dataset D	Stem (cylindrical)	0	8	8
	Leaf (slice)	0	8	8
Total		75	51	126

point clouds:

$$D(\bar{X}, s) = \begin{cases} 0.1 & \bar{X} = (\pm s, 0, 0) \text{ or } (0, \pm s, 0) \text{ or } (0, 0, \pm s) \\ 0.4 & \bar{X} = (0, 0, 0) \\ 0 & \text{Otherwise} \end{cases} \quad (21)$$

In addition, in order to evaluate the performance of our proposed method on noisy point clouds captured in real-world by different ways, we requested 12 maize point clouds from Miao et al. (2022) and 8 maize point clouds from Wu et al. (2020), which were collected using a Trimble tx8 TLS terrestrial laser scanner in the field and the MVS technique indoors, respectively. The ground points and the outlier points were manually removed using the statistical filtering algorithm in PCL, respectively. The processed point clouds were then used as input for noise point clouds for our method and baseline methods, and the denoising performance of the network was evaluated visually.

4.2. Network training and testing

All experiments in this study were conducted on the same computer, which includes an Intel Core (TM) i7-10700F CPU, and a NVIDIA GeForce GTX 1650 GPU with 4 GB memory. The operating system was Ubuntu 18.04. As the hyper-parameters for training our proposed PDN, the batch size was set to 16, the initial learning rate was set to 0.0002, and the Adam solver was used as the optimizer of network training. For other baselines methods, we kept the original parameter settings and only modified the batch size to fit our GPU memory. All networks were properly trained until the loss remained unchanged, and the network parameters with the lowest loss were selected.

As for high-throughput plant phenotyping, the efficiency of the algorithm is crucial. Therefore, we qualitatively compare our proposed method and baseline methods in terms of their runtime performance, network complexity, and denoising performance.

4.3. Baselines

Popular and state-of-the-art deep-learning-based denoising networks including PCN, DMR, and SD were selected for comparison. SD was the most advanced model in denoising performance before this work. PCN and SD use an iterative approach when dealing with point clouds with high noise level, i.e., the network's output point cloud is re-input into the network as the noisy point cloud to achieve higher denoising performance. Therefore, for these two baselines, multiple iterations were performed and the final results with the highest denoising performance were selected.

4.4. Evaluation metrics

In this study, Chamfer Distance (CD) (Fan et al., 2017) was used as the metric to evaluate different methods. CD is a metric widely used to evaluate the similarity between two point clouds. Let P_{gt} be the ground truth (clean) point cloud of the input neural network's noisy point cloud, and P_o be the output point cloud of the neural network, then the CD was defined as:

$$CD(P_o, P_{gt}) = \frac{1}{|P_o|} \sum_{q \in P_o} \min_{p \in P_{gt}} \|q - p\|_2 + \frac{1}{|P_{gt}|} \sum_{p \in P_{gt}} \min_{q \in P_o} \|p - q\|_2. \quad (22)$$

where the first term in the formula calculates the sum of the minimum distance from each point in the output point cloud to the ground truth, and the second term calculates the sum of the minimum distance from each point in the ground truth point cloud to the output point cloud.

5. Results

5.1. Denoising performance on Gaussian noise

As described in Section 4.1, models were trained using maize point clouds perturbed by Gaussian noise. This section aims to demonstrate the robustness of our model in handling Gaussian noise and its ability to generalize to other plant species. Firstly, we compared the denoising performance of three baselines with our proposed model on maize point clouds from Dataset A at different levels of Gaussian noise (Table 2). Our results outperformed all baselines at all noise levels. Our method achieved a relative improvement of 10.6 % to 19.3 % compared to SD at different noise levels, achieving state-of-the-art denoising performance.

Fig. 5 shows the visual comparison of the denoising results of different denoising methods on maize point clouds with 1 % Gaussian noise level. It can be observed that our method output point clouds closer to the clean point cloud than other methods and preserved the details of the point cloud well. DMR struggled to learn the potential surface representation of noisy point clouds when processing complex plant point clouds, leading to larger surface reconstruction errors, which also resulted in larger errors in during resampling on the reconstructed surface. PCN almost showed no denoising effect on sparse noisy point clouds, while on dense noisy point clouds, outliers and shrinkage were observed. The denoising result of SD was the best among all baselines, without the issues of outliers and shrinkage, but it failed to preserve the details.

Furthermore, with the baselines and our model trained only on maize point clouds, we conducted quantitative comparisons of their denoising performance on Gaussian noise-perturbed point clouds of four other species, including Arabidopsis, tobacco, tomato, and sorghum from Dataset B, in order to demonstrate the generalization capability of our model in denoising point clouds of plants of different species. Our results outperformed the other baselines when applied on point clouds of other plant species with different levels of Gaussian noise (Table 2). Our method achieved a relative improvement of 7.6 % to 16.7 % compared to SD at different noise levels, still achieving state-of-the-art denoising performance. DMR and PCN have poor generalizability, as their denoising performance decreased when transferred to point clouds of other plant species. SD and our method both maintained good generalization ability, and our results achieved better performance than SD.

Fig. 6 shows the visual comparison of the denoising results of some other plants test samples under 1 % Gaussian noise level. It can be seen that our denoising results are closer to the clean point clouds of all species, including Arabidopsis, tobacco, and tomato, whose morphology is significantly different from maize and sorghum.

5.2. Denoising performance on different types of noise

Besides Gaussian noise, other types of noise such as Laplace noise, uniform noise, and discrete noise are also commonly included in point

Table 2

Quantitative comparisons of different point cloud denoising methods using the maize and other plants test point clouds synthesized by Gaussian noise of different noise levels.

Species	Model	CD (10^{-4})			
		Noise level @0.5 %	Noise level @1%	Noise level @1.5 %	Noise level @2%
Maize	DMR	2.714	2.701	3.150	4.049
	PCN	0.698	1.405	2.576	4.565
	SD	0.740	1.151	1.978	2.880
	Ours	0.612	1.029	1.597	2.513
Other Plants	DMR	4.511	4.348	4.201	4.541
	PCN	0.805	1.507	2.611	4.547
	SD	0.777	1.098	1.675	2.423
	Ours	0.647	1.015	1.409	2.117

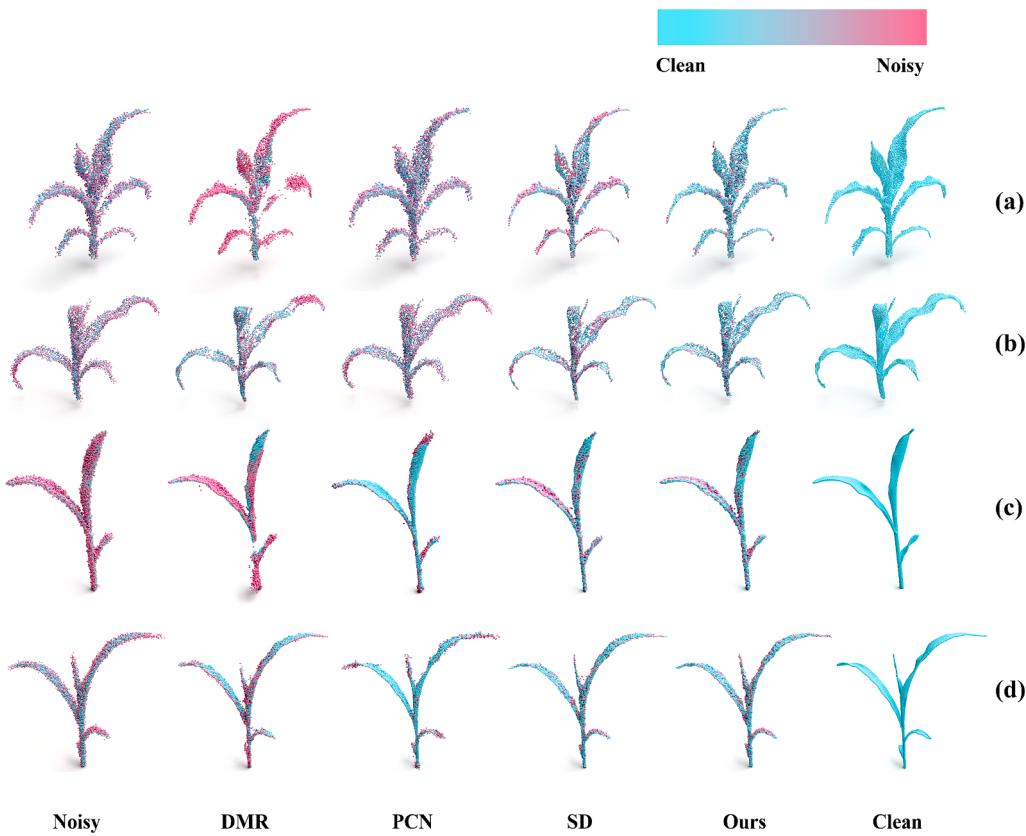


Fig. 5. The visualization comparison of point cloud denoising methods on the maize test samples perturbed by Gaussian noise at a level of 1%. (a) and (b) show the denoising results of sparse noisy point clouds, while (c) and (d) show the denoising results of dense noisy point clouds. The point numbers for (a)-(d) are 5340, 5157, 8432, and 10350, respectively. The color represents the error between the point and the underlying clean surface, i.e. the distance between the point and the underlying clean surface. Points closer to the underlying clean surface were colored pinker, otherwise colored bluer.

clouds collected in real world. The purpose of this section is to demonstrate that our model still has superior denoising performance for other types of noise. Table 3 shows the denoising performance of different point cloud denoising methods on the maize point clouds from Dataset A, perturbed by Laplace noise, uniform noise and discrete noise. In terms of Laplace noise, the denoising performance of our model was better than the baselines at most noise levels except for high noise levels (2 %), with which the Laplacian noise point cloud contains many outliers. Our model had difficulty in estimating the density gradient of these points, resulting in unsatisfactory denoising performance. DMR effectively removed outliers by resampling on the reconstructed surface, thereby achieved better denoising results. In terms of uniform noise and discrete noise, our results were better than the baselines at most noise levels, except for low noise levels, at which our model slightly underperforms the PCN method.

The visual comparison of denoising results of point cloud denoising methods on the maize test samples perturbed by other types noise is shown in Fig. 7. It can be seen that our denoising outputs were superior to the baselines, which were closer to the clean shape of the maize than the baselines, without causing shrinkage.

5.3. Denoising performance on point clouds with varying density and various geometric shapes

In 3D phenotyping applications, the collected plant point clouds often exhibit uneven density and incompleteness, and some 3D phenotyping methods process point clouds of plant organs separately to extract more precise plant structural phenotypes. This section aims to demonstrate the denoising performance of the proposed method in plant point clouds with uneven density and incompleteness, as well as point clouds

of plant organs with specific geometric features. Denoising results on maize point clouds with uneven density and incompleteness (from Dataset C), leaf point clouds, and stem point clouds (from Dataset D), perturbed by Gaussian noise, are presented in Table 4. In terms of maize point clouds with uneven density and incompleteness, our results generally surpass the baselines at most noise levels. While DMR and PCN show good denoising performance in densely populated areas of point clouds, they encountered challenges in sparse and incomplete regions due to difficulties in accurately constructing geometric features of potential surfaces, leading to inaccurate denoising displacement predictions. SD and the proposed method, both relying on density gradient estimation, exhibited robust performance in handling situations with uneven density and incompleteness in plant point clouds. However, the proposed method, which employed a feature fusion module, achieved estimation of density gradients with higher precision, therefore effectively mitigated the issue of hole expansion (Fig. 8). This demonstrates the proposed methodology has superior denoising performance and adaptability to the inherent flaws in data used in phenotyping applications, including the uneven density and incompleteness.

In terms of point clouds of plant organs, performance decline was observed on the tested algorithms (Table 4). This is because the models were trained or tuned using point clouds of whole plants, whereas leaves and stems possess distinct geometric features (for instance, stems exhibit cylindrical characteristics) from the plant point clouds and lack complex structures. It is observed that our proposed method generally outperform the baselines across most noise levels. As the baseline methods, DMR, which relies on potential surface learning for denoising, struggles to adapt to the domain shift, resulting in a substantial decline in denoising performance compared to the maize point clouds. PCN exhibits poor denoising performance on leaves. SD and our proposed

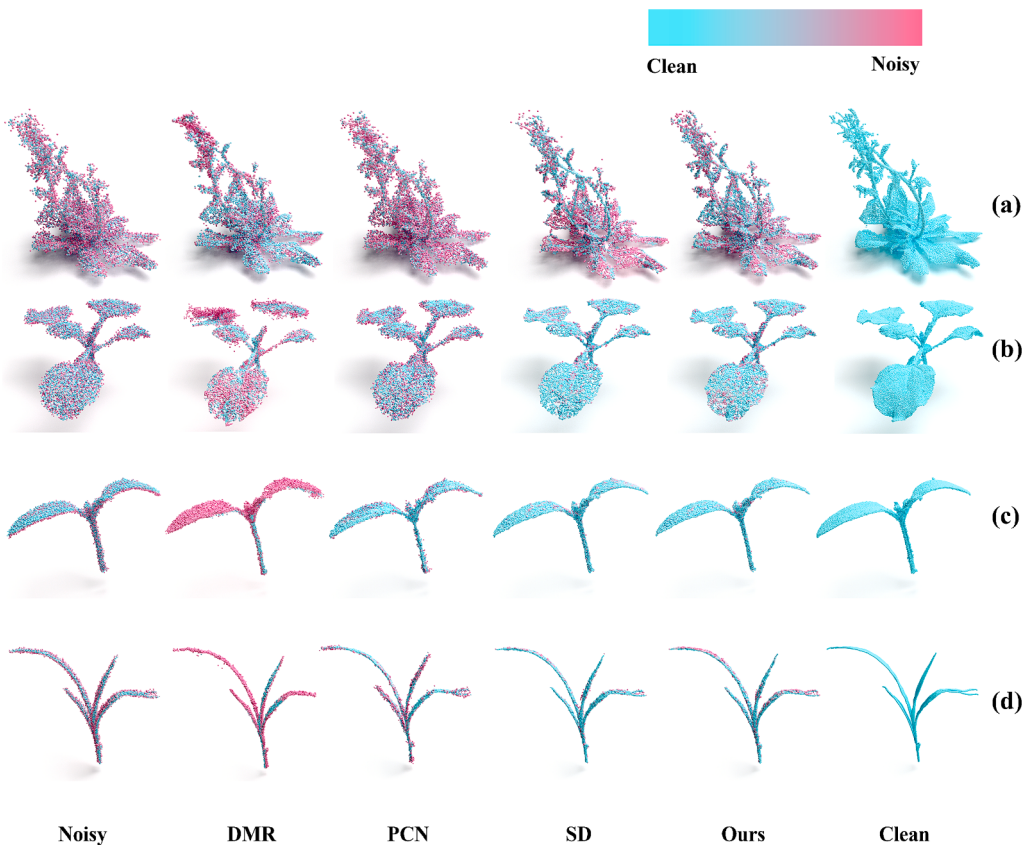


Fig. 6. The visual comparison of the denoising results of other plants test samples perturbed by Gaussian noise using point cloud denoising methods, with a noise level of 1%. (a) Arabidopsis (b) tomato (c) tobacco (d) sorghum.

Table 3

Quantitative comparison of denoising results of point cloud denoising methods on maize test set perturbed by other types noise.

Noise type	Model	CD (10^{-4})			
		Noise level @0.5 %	Noise level @1%	Noise level @1.5 %	Noise level @2%
Laplace	DMR	2.635	2.800	3.471	4.751
	PCN	0.906	2.306	5.050	9.219
	SD	0.857	1.870	3.692	7.597
	Ours	0.705	1.521	3.200	6.478
Uniform	DMR	2.808	2.804	2.831	2.826
	PCN	0.285	0.670	0.981	1.306
	SD	0.645	0.730	0.843	1.001
	Ours	0.458	0.606	0.737	0.928
Discrete	DMR	2.808	2.773	2.660	2.736
	PCN	0.270	0.570	0.794	1.058
	SD	0.633	0.712	0.816	1.002
	Ours	0.432	0.554	0.643	0.803

method both maintained good denoising performance, and our proposed method has better performance than SD in stem point clouds (Fig. 9). This demonstrates the adaptability of the proposed methodology to organ-level plant phenotyping applications.

5.4. Visual evaluation with real-world noisy point clouds

The purpose of this section is to assess the denoising effectiveness of our method on point clouds with varying densities, incompleteness, and noise, which were acquired from real-world scenarios. Maize point clouds collected in the experimental field and indoors were preprocessed to remove ground points and outliers, and used as input noise point clouds for the baselines and our method. Since these is no corresponding

ground truth point clouds for these point clouds, the denoising performance was only evaluated and compared visually. The denoising results of different models are shown in Fig. 10.

The original point clouds collected in the field were uneven density and incomplete, contained high level noise, which contributes to unevenness on the surface of the point clouds, and appears as dark color in point cloud visualization (Fig. 10 (a), (b)). The raw point cloud collected indoors through MVS technology exhibits low noise in homogeneous regions, but there is a higher level of noise at the edges of leaves, attributed to spatial edge noise generated at the intersection of foreground and background (Fig. 10 (c), (d)). After denoised by our proposed method, the surface of the point cloud became smooth and the color becomes brighter in visualization. Comparing with other baseline methods, our proposed method output point clouds with smoother surfaces and lower noise level. The morphological features of maize were better preserved as well, which were more compatible with existing morphological phenotype extraction algorithms, such as the cylinder fitting algorithm to approximate the real stem shape, as well as the surface reconstruction algorithm to reconstruct a leaf surface in extracting the morphological phenotypes of plants. Among the baseline methods, DMR performed poorly on the actually collected point cloud and deteriorated regions that were initially low in noise (Fig. 10 (c), (d)). This is due to the disparity between the learned potential surface representation and the actual surface representation. PCN struggles to address spatial edge noise and performs poorly on highly noisy point clouds. Although SD achieved a similarly high performance in noise removal comparing to our proposed method, it was less effective in preserving the local features of the point clouds, which created some holes and more outliers, whereas our proposed method made the spatial distribution of the point clouds more uniform.

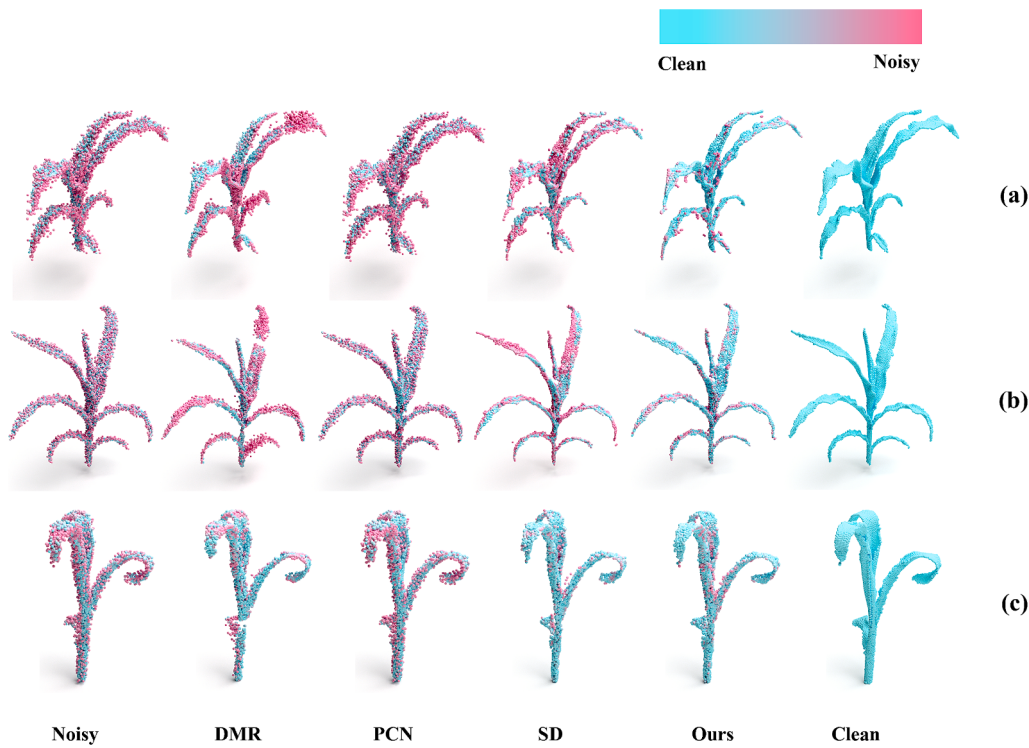


Fig. 7. The visual comparison of denoising results of maize test samples perturbed by other noise types using point cloud denoising methods. (a) shows the denoising results of Laplacian noise point clouds, with a noise level of 1%. (b) shows the denoising results of uniform noise point clouds, with a noise level of 2%. (c) shows the denoising results of discrete noise point clouds, with a noise level of 2%.

Table 4

Quantitative comparison of denoising results of different methods on Gaussian noise-perturbed point clouds, including maize point clouds with uneven density and incompleteness (Dataset C), as well as cropped leaf and stem point clouds (Dataset D).

Point cloud type	Model	CD (10^{-4})			
		Noise level @0.5 %	Noise level @1%	Noise level @1.5 %	Noise level @2%
Maize (uneven density and incompleteness)	DMR	0.917	1.116	1.745	2.664
	PCN	0.226	0.577	1.592	2.443
	SD	0.218	0.512	1.024	1.753
	Ours	0.182	0.444	0.957	1.754
Leaf (slice feature)	DMR	4.423	4.823	5.217	5.894
	PCN	0.627	1.135	2.058	3.868
	SD	0.464	0.656	0.897	1.233
	Ours	0.448	0.634	0.899	1.247
Stem (cylindrical feature)	DMR	1.757	1.846	2.224	2.928
	PCN	0.477	0.801	1.670	3.627
	SD	0.487	0.913	1.669	2.272
	Ours	0.421	0.741	1.334	2.051

5.5. Network complexity and runtime performance

The runtime performance, network complexity, and denoising performance of our proposed method and the baseline methods were qualitatively compared (Table 5). As the result, our proposed algorithm achieves the best runtime performance at all noise levels whereas the least network complexity. Compared with SD, which has comparable performance to our proposed method, our proposed model improved the efficiency by 0.5–8.6 times, and the number of parameters was only about half of SD.

6. Discussion

6.1. Effect of the hyper-parameter K

In our proposed PDN, **k-NN algorithm** was used in different modules including PDF extraction, UOF calculation. The K value represents the number of neighbors to inspect in neighbor searching, which indirectly controls the extent of the local surface where the point is situated. Therefore, it affects the extracted PDF, UOF, and subsequently calculated point density gradient. In order to explore the optimal K value for PDN, a parameter tuning experiment was designed.

16 versions of PDN with K value as an independent variable were trained and tested (Fig. 11). The step size of K was 2, and the range was 2–32. It can be seen that a K value that is either too large or too small caused a decrease in network performance. This is because a small K value makes the network difficult to extract PDF, and decreased the correlation between UOF and density gradient direction. A large K value also reduces the correlation between UOF and density gradient direction, especially in regions with large surface curvature changes. Since PDN achieves the best denoising performance for most noise levels at K = 18, K = 18 was selected in this study.

6.2. Ablation analysis

The proposed method mainly includes a PDF extraction module, a UOF calculation module, and a point DG estimation module. We conducted ablation studies on these three main modules to assess the contribution of the proposed method's main design:

A. PDF extraction module

With this module, the point coordinates were encoded into PDFs. The PointNet (Qi et al., 2017a) point feature encoder, with a comparable number of layers and parameters to the PDF extraction module, was

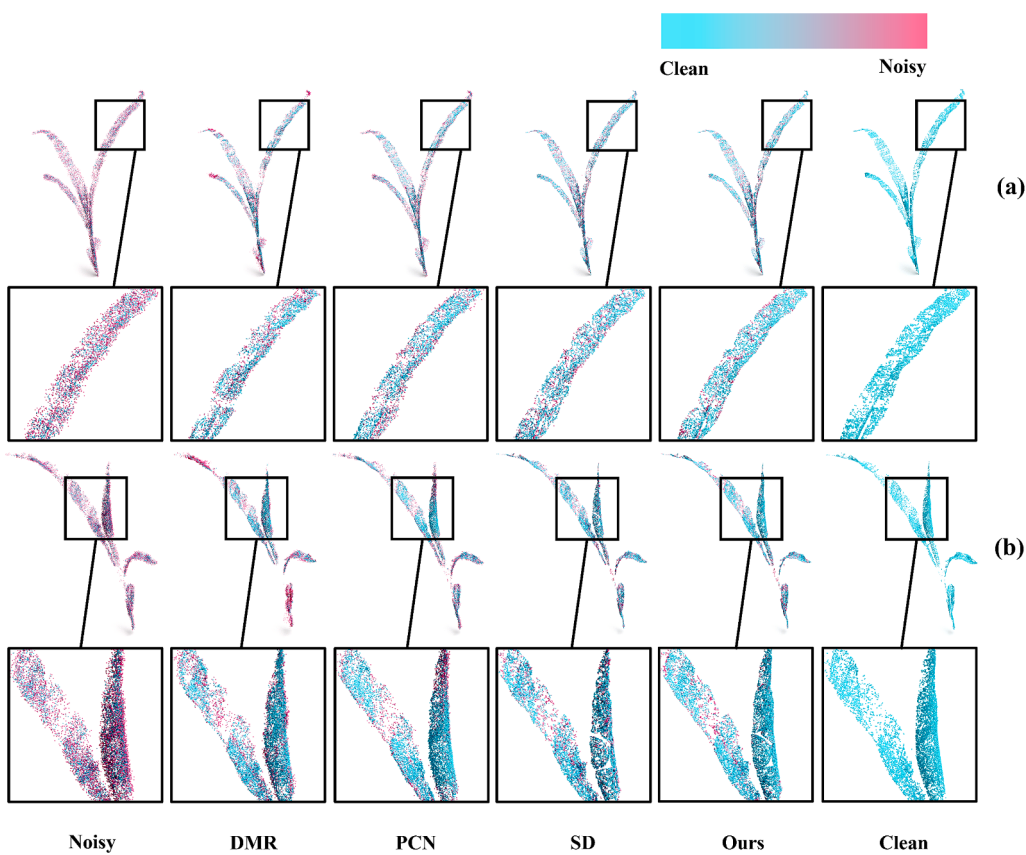


Fig. 8. The visual comparison of denoising results of uneven density and incompleteness maize test samples perturbed by Gaussian noise using point cloud denoising methods.

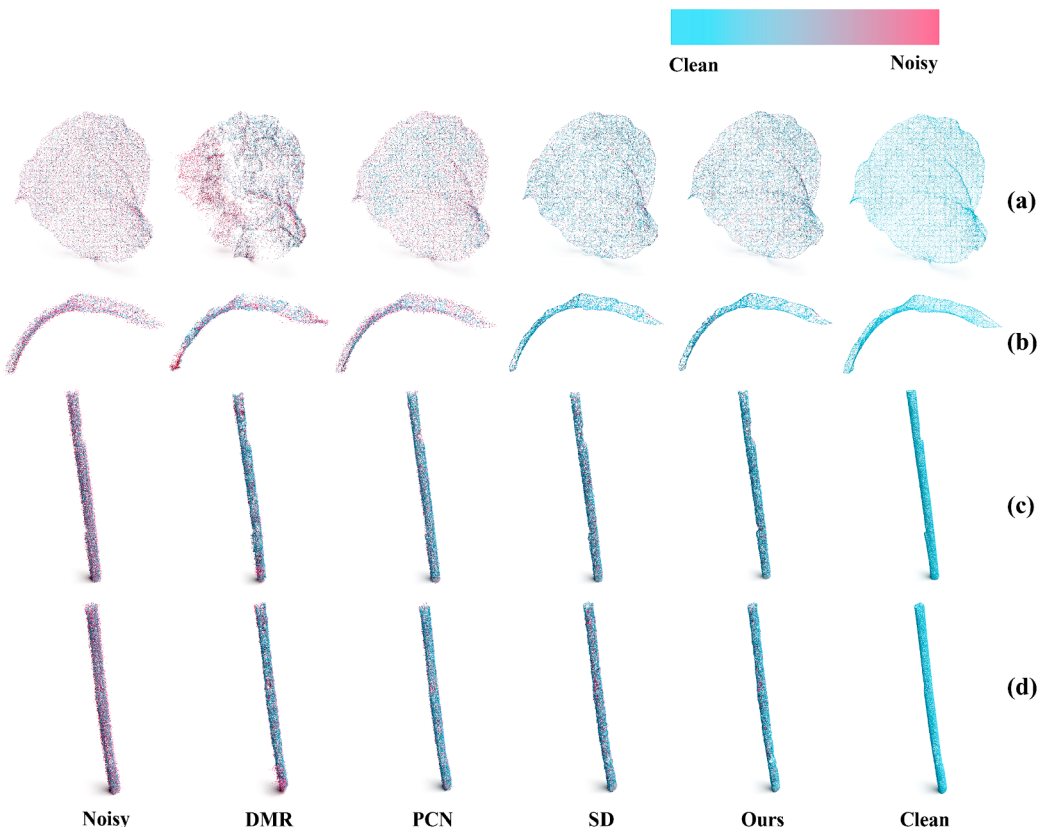


Fig. 9. A visual comparison of denoising results from different denoising methods on point clouds of leaves and stems, perturbed by Gaussian noise.

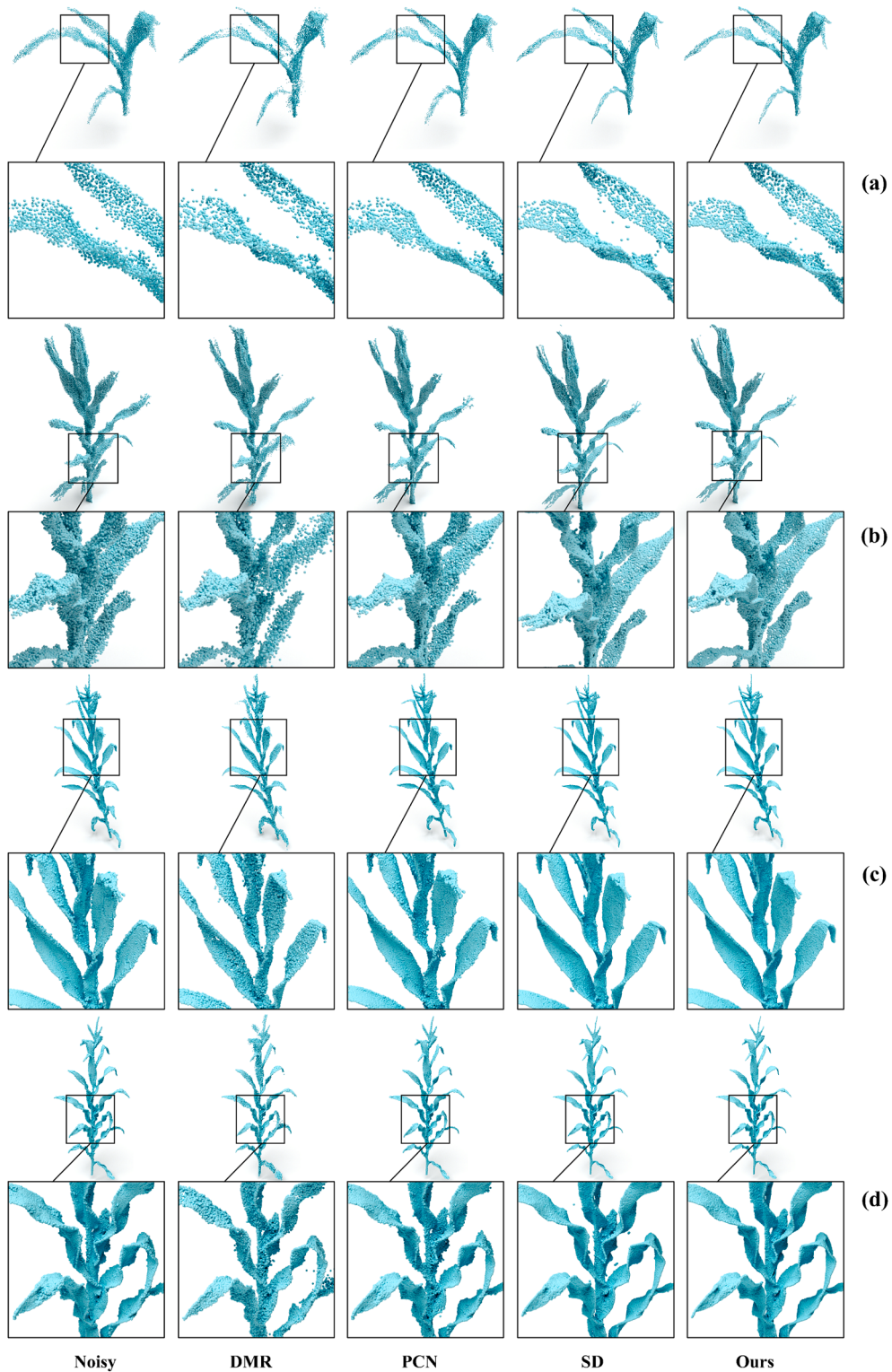


Fig. 10. The visual comparison of denoising results of different point cloud denoising methods using field-collected point clouds((a), (b)) and indoors-collected point clouds((c), (d)).

employed to substitute the PDF extraction module in this ablation study. The point features extracted by the PointNet point feature encoder were integrated with UOF and input into the DG estimation module.

B. UOF calculation module

This module calculates an umbrella operator for each point in the

point cloud. Removing the UOF calculation module is equivalent to removing the UOF in feature fusion within DG estimation module. Therefore, we directly fed the point density features into the point DG estimation module.

C. Point DG estimation module

Table 5

Quantitative comparison of runtime performance, number of iterations and network complexity of different point cloud denoising methods on maize point clouds.

Model	Noise level @0.5 %		Noise level @1%		Noise level @1.5 %		Noise level @2%		Num. Params/M
	Time /s	Iterations	Time /s	Iterations	Time /s	Iterations	Time /s	Iterations	
DMR	1.324	0	1.270	0	1.292	0	1.329	0	0.22
PCN	127.6	2	114.9	2	128.1	2	124.8	2	27.95
SD	0.849	2	2.747	15	5.811	32	6.967	40	0.19
Ours	0.578	0	0.579	0	0.642	1	0.723	2	0.10

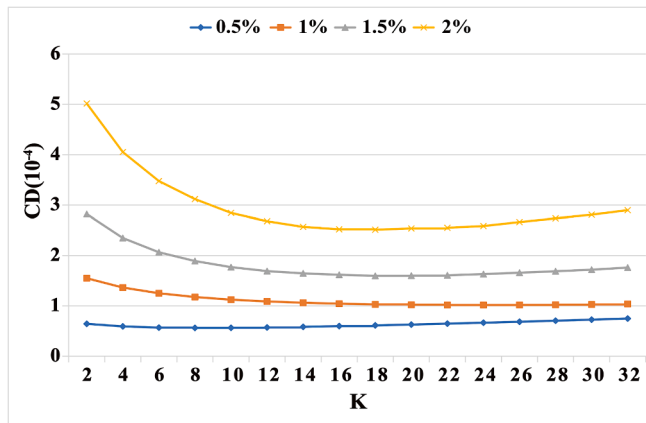


Fig. 11. Parameter tuning of the hyper-parameters K of PDN.

The point DG estimation module maps the fused features of the points to the density gradient of the points, achieving a transformation from feature space to 3D space. It features an MLP structured with residuals. In ablation analysis, the residual connection of the DG was disengaged, which transformed it into an MLP with equivalent network layers and parameters.

The quantitative results are shown in Table 6. Removing any of the modules led to a decrease in network denoising performance, indicating that the main modules of the proposed method contributed to the final results. The visual comparison of denoising results in the ablation study is shown in Fig. 12. Substituting the PDF extraction module with the PointNet point feature encoder diminishes the network's ability to capture point density features, as the PointNet point feature encoder having a less robust capability to extract local spatial features compared to EdgeConv. This led to difficulties in moving the noisy point cloud to the regions with the highest density, resulting in the denoised point cloud being further away from the potential surface, visually appearing more bloated than the original point cloud (Fig. 12 (A)). The absence of the umbrella operator feature calculation module in the network reduced the capability of classifying the density gradient of outliers, resulting in inaccurate movement directions of these points. Visually, the denoised point cloud contained outliers farther away from the underlying surface (points with pinker colors in Fig. 12 (B)). Breaking the residual connection of the point DG estimation module would hinder the

network's ability to estimate point density gradients, thereby impeding the denoising process (Fig. 12 (C)). This is attributed to the deep network structure of point DG estimation module, residual connection. the problem of gradient vanishing arises, hindered the convergence of the network.

6.3. Phenotype extraction

The purpose of this section is to discuss the impact of our algorithm on the extraction of plant 3D phenotypes. We used the automatic maize plant phenotypic extraction method designed by Miao et al. (2021) to extract plant phenotypes from the noisy point cloud and the point cloud denoised by our proposed PDN. The stem and leaves were extracted as the skeleton of the plant point cloud (Cao et al., 2010), Then morphological phenotypes including plant height, crown diameter, leaf length and width, stem diameter and length were extracted. The segmented leaves were reconstructed using Meshlab software, then the leaf area was calculated. The entire phenotypic extraction process is shown in Fig. 13.

10 maize point clouds with 0.5 % Gaussian noise level were processed to extract the phenotypes, and the ground truth of these phenotypes were manually measured from noise-free point clouds using CloudCompare software. As the number of leaves on these maize point clouds was different, we summed all leaf phenotypes (length, width, and area) extracted from the same maize point cloud as the leaf phenotype of the maize point cloud for statistical analysis. Fig. 14 shows the correlation analysis between the extracted phenotypes and the manually measured phenotypes using noisy point clouds and point clouds denoised by PDN. It can be seen that the phenotypes extracted using point clouds denoised by PDN have a high correlation with the manually measured phenotypes, with a correlation coefficient R^2 between 0.8445 and 0.9999, and the RMSE is lower than the phenotypes extracted using noisy point clouds, especially for structural phenotypes such as leaf area and stem diameter.

The leaf surface reconstruction results using the raw noisy data, the ground truth clean data, and the PDN-output data were compared visually (Fig. 15). The surface reconstructed from the noisy point cloud has greater roughness and appears as an enclosed shell structure overall, which leads to a greater leaf area than the ground truth. In terms of leaf area measurement, the leaf area extracted from the noisy point cloud is almost twice of the ground truth. In contrast, the surface reconstructed from the point cloud denoised by PDN is relatively smoother and appears as a thinner slice overall, which leads to a more accurate measurement of leaf area.

6.4. Compare with SD

SD performs gradient ascent using estimated gradients of each point based on the probability density. However, in phenotyping applications, the plant point clouds are diverse in species and noise types, and often present challenges such as uneven density and incompleteness, which leads to inaccurate density gradient estimation of SD. Consequently, it must rely on smaller gradient ascent steps and multiple iterations to ensure denoising performance, resulting in lower efficiency. The new

Table 6

Quantitative comparison of denoising results of the ablation study of PDN.

Species	A	B	C	CD (10^{-4})				
				Noise level @0.5 %	Noise level @1%	Noise level @1.5 %	Noise level @2%	
Maize	✓	✓	✓	0.687	1.149	1.839	2.704	
	✓	✓	✓	0.625	1.088	1.671	2.585	
	✓	✓	✓	0.783	1.841	3.307	5.218	
	✓	✓	✓	0.612	1.029	1.597	2.513	

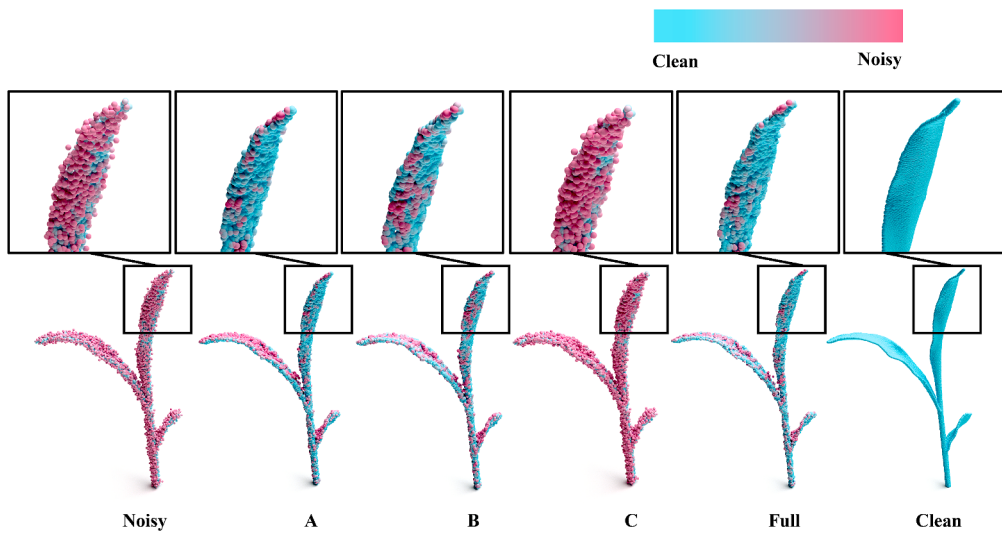


Fig. 12. Visualization comparison of the denoising results of ablation experiments. (A) the denoising result of PDN when replace the PDF extraction module with PointNet point feature encoder; (B) the denoising result of PDN when the UOF calculation module is missing; (C) the denoising result of PDN when the residual connection of point DG estimation module was broken; (Full) the denoising result of PDN without any missing module.

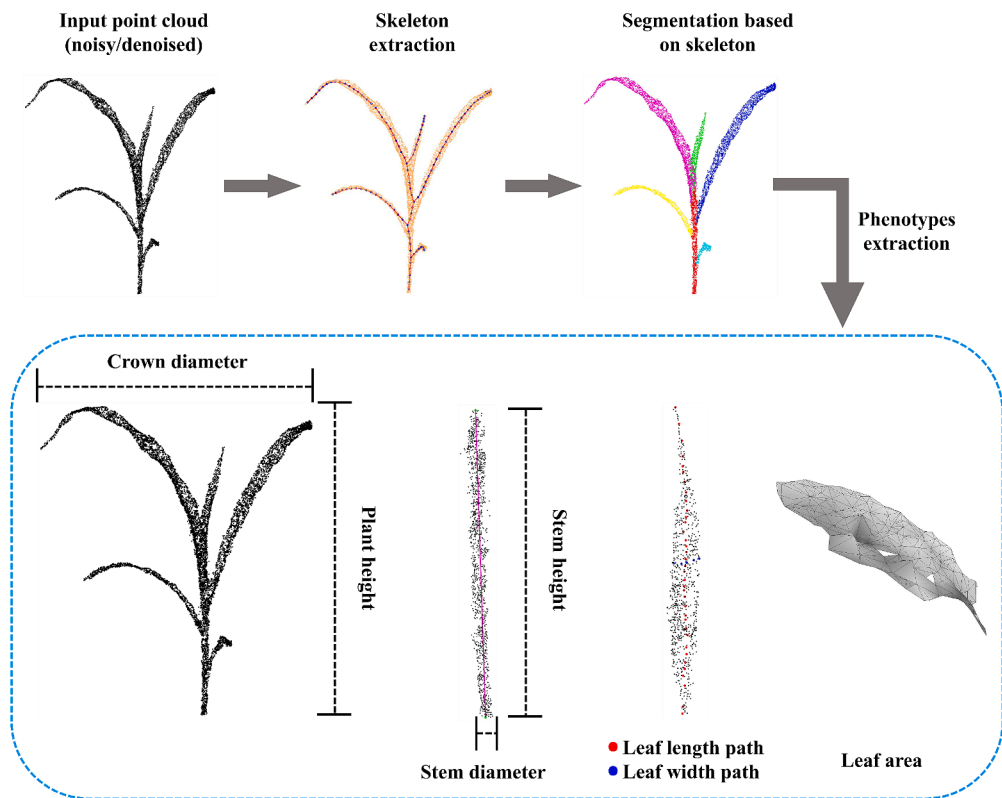


Fig. 13. The process of phenotype extraction.

framework we proposed used the concept of gradient ascent similar to SD, but it employed feature fusion to encode point density features, allowing for a more precise estimation of density gradients. This enables the proposed method to denoise the cloud at once during gradient ascent, eliminating the need for additional iterations and improving processing efficiency while maintaining better denoising performance.

During gradient ascent, SD can reduce the number of iterations and improve algorithm efficiency by increasing the step size α in Equation (12), at the cost of performance decreases (Fig. 16). This is because an excessively large step size can lead to excessive contraction, as the

calculated displacement of the points may exceed the distance from noise points to the potential surface. By comparing the denoising performance of SD at various step sizes, it is observed that when the step size $\alpha = 0.2$, the denoising performance approached the optimal value without experiencing excessive contraction. Therefore, a step size of $\alpha = 0.2$ was used for all tests about SD. When $\alpha = 1$, it means updating all gradients to the noisy point cloud during gradient ascent. By comparing the denoising performance of SD and the proposed method at $\alpha = 1$, it is evident that the proposed method can more accurately estimate the density gradients to eliminate iterations and keep better denoising

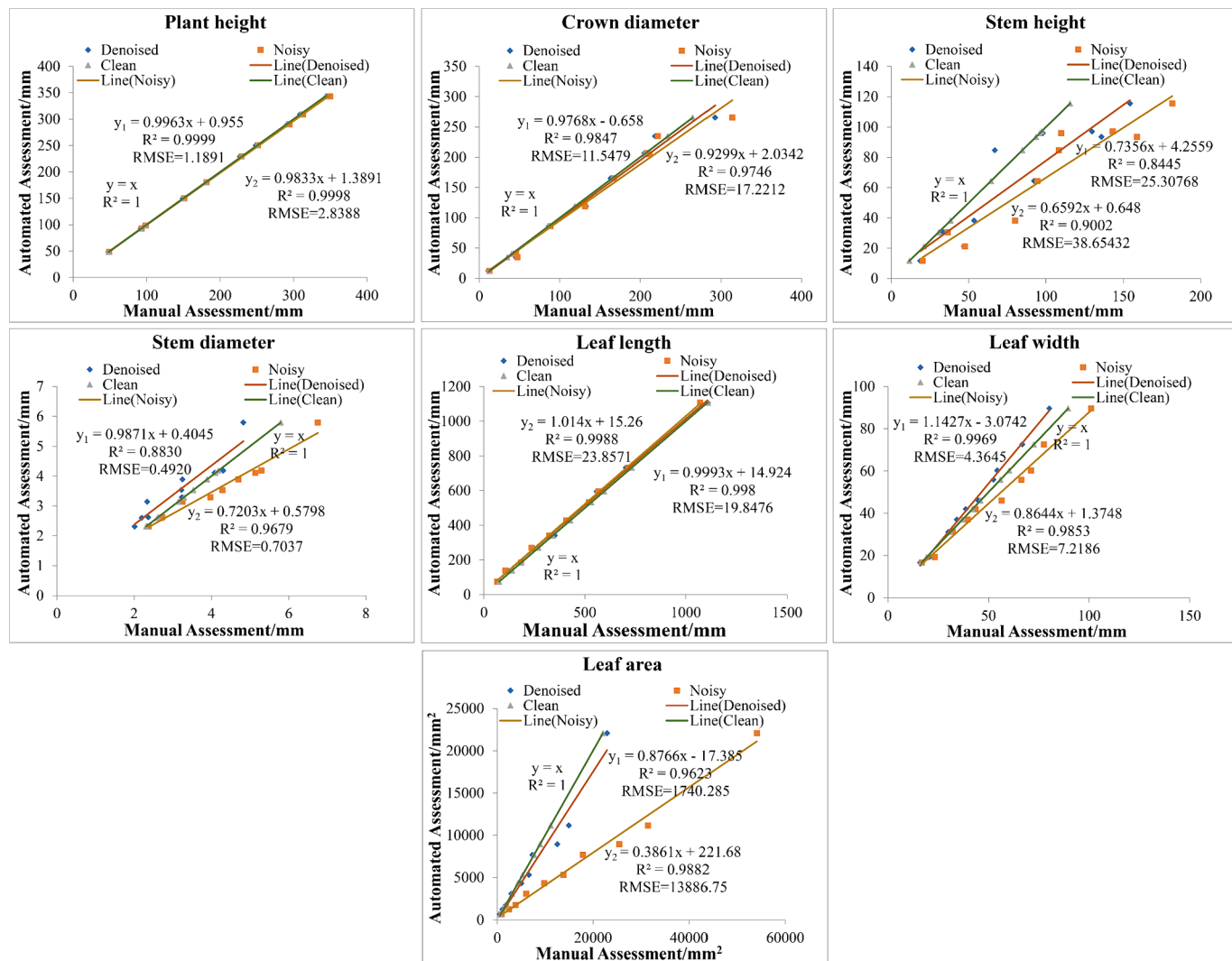


Fig. 14. Correlation analysis of maize phenotypes. A total of seven phenotypes including plant height, canopy diameter, stem height, stem diameter, leaf length, leaf width, and leaf area were analyzed. The deep green line is the ideal regression line ($y = x$), the deep orange line is the least squares regression line of phenotypes extracted using point clouds denoised by PDN, and the deep gold line is the least squares regression line of phenotypes extracted using noisy point clouds. (For interpretation of the references to color in this figure legend, the reader is referred to the web version of this article.)

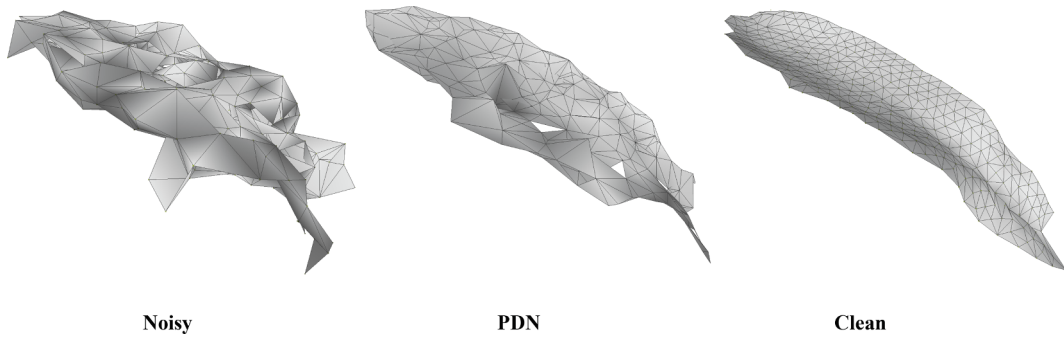


Fig. 15. The visual comparison of the leaf surface reconstruction results.

performance, so a step size of $\alpha = 1$ was used for all tests about PDN.

Along with the experimental results comparing the denoising performance and processing efficiency between the proposed method and various baseline methods, including SD, it has been demonstrated that the main advantage of the proposed approach lies in its enhanced ability to accurately estimate point density gradients. This not only enhances

the efficiency of gradient ascent but also leads to superior denoising performance compared to SD. Therefore, this method emerges as a more promising tool for denoising plant point clouds.

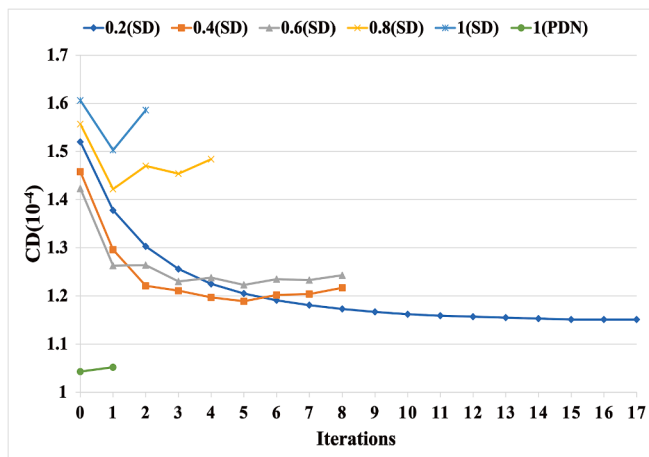


Fig. 16. The variation in denoising performance and iterations for SD and PDN with different step sizes at 1% Gaussian noise level.

6.5. Compare with smoothing methods

Some smoothing algorithms can effectively smooth the point cloud of the leaves to obtain a continuously smooth surface to represent the leaves surface. We conducted a simple test on the most commonly used smoothing algorithm for leaves, the Moving Least Squares (MLS) algorithm, as shown in the Fig. 17. It can be seen that, compared to the proposed denoising method, the MLS algorithm can obtain a smoother and more uniform surface but fails to preserve some detailed features of the point cloud (such as leaves edges) and causes excessive smoothness in some areas. The rationale behind this phenomenon lies in the inherent objective of smoothing algorithms, which is to approximate a smooth and continuous surface over the point cloud and subsequently sample points from it. Consequently, this process results in the attenuation of intricate features within the point cloud. Notably, this contradicts the denoising concept, whose primary goal is to reinstate the original shape of the point cloud while safeguarding essential detailed features. Preserving these features proves critical for subsequent stages of point cloud processing.

7. Conclusion

3D High-throughput plant phenotyping methods face a dual challenge of high throughput and high accuracy. Current off-the-shelf denoising methods cannot guarantee the efficiency and accuracy at the same time when processing plant point clouds. In this paper, we proposed a plant point cloud denoising network which predicts the density gradient (DG) of noisy point clouds. It can effectively alleviate the challenges posed by uneven density, incompleteness, diverse species, varying noise types, and the large data volume of plant point cloud. Experimental results show that under different noise levels, our method has a relative improvement rate of 10.6 %–19.3 % in terms of denoising performance compared to the state-of-the-art methods, achieving state-of-the-art denoising performance. In terms of processing speed, with noise level from 0.5 % to 2 %, the runtime for processing 10,000 points ranged from 0.578 s to 0.723 s for our proposed method, which is more than 0.5–8.6 times faster than state-of-the-art methods with comparable performance, meeting the real-time requirements. Therefore, our proposed point cloud denoising algorithm is effective and suitable for high-throughput plant 3D phenotype methods, and may promote high-throughput and high-precision phenotype extraction in plant 3D phenotyping.

Since the denoising network proposed in this paper is based on the prediction of point density gradient, the estimation of point density gradient becomes challenging when the noisy point cloud is sparse or has uneven density, leading to a decrease in denoising performance. In the future, our work will primarily focus on two aspects: firstly, designing a density variation-based local neighborhood extraction algorithm, which performs a fixed-radius search for the nearest neighbors. Since the number of the nearest neighbors around the center point is not a fixed value, the challenge will be to design a neural network as a feature aggregator to process neighbor feature vectors with varying length. Secondly, we observed that most denoising methods including SD using the gradient ascent strategy demand iterations during testing, in an asymptotically optimal manner especially at higher noise levels, despite the absence of consideration for iterations during training. We are currently developing an iterative denoising network, which will factor in the loss at each iteration, aiming to learn the most effective iteration strategy and enhance overall denoising performance, therefore solves the problem of poor denoising performance due to inconsistency.

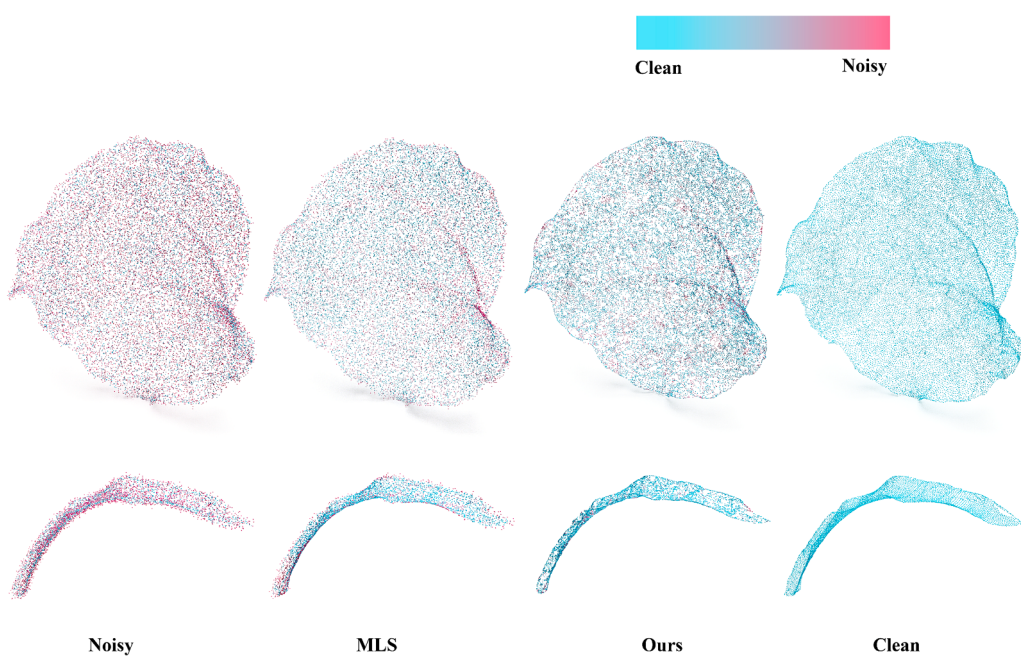


Fig. 17. The visual comparison of the smoothing method MLS and the proposed denoising method.

between training and testing with high noise levels.

CRediT authorship contribution statement

Jianeng Wu: Methodology, Software, Data curation, Formal analysis, Validation, Visualization, Writing – original draft, Writing – review & editing. **Lirong Xiang:** Methodology, Investigation, Validation, Writing – review & editing. **Hui You:** Conceptualization, Methodology, Funding acquisition, Writing – review & editing. **Lie Tang:** Conceptualization, Resources, Writing – review & editing. **Jingyao Gai:** Conceptualization, Methodology, Supervision, Project administration, Funding acquisition, Writing – review & editing.

Declaration of competing interest

The authors declare that they have no known competing financial interests or personal relationships that could have appeared to influence the work reported in this paper.

Acknowledgements

This project was funded by National Natural Science Foundation of China, China (Award No.: U23A202599) and Specific Research Project of Guangxi for Research Bases and Talents, China (Award No.: AD22035919). This research is also a product of the Modern Industry School of Subtropical Intelligent Agricultural Machinery and Equipment, Guangxi University, China, Project No. T3010097930. We thank Dr. Zhang Man from China Agriculture University for sharing their data for the development and evaluation of our proposed method.

References

- Ao, Z., Wu, F., Hu, S., Sun, Y., Su, Y., Guo, Q., Xin, Q., 2022. Automatic segmentation of stem and leaf components and individual maize plants in field terrestrial LiDAR data using convolutional neural networks. *The Crop Journal* 10 (5), 1239–1250. <https://doi.org/10.1016/j.cj.2021.10.010>.
- Boogaard, F.P., van Henten, E.J., Kootstra, G., 2022. Improved point-cloud segmentation for plant phenotyping through class-dependent sampling of training data to Battle class imbalance. *Front. Plant Sci.* 13 <https://doi.org/10.3389/fpls.2022.838190>.
- Boukhana, M., Ravaglia, J., Hétroy-Wheeler, F., De Solan, B., 2022. Geometric models for plant leaf area estimation from 3D point clouds: a comparative study. *Graphics and Visual Computing* 7, 200057. <https://doi.org/10.1016/j.gvc.2022.200057>.
- Cao, J., Tagliasacchi, A., Olson, M., Zhang, H., Su, Z., 2010. Point cloud skeletons via laplacian based Contraction. *Shape Modeling International Conference* 2010, 187–197. <https://doi.org/10.1109/SMI.2010.25>.
- Casajus, P.H., Ritschel, T., Ropinski, T., 2019. Total denoising: unsupervised Learning of 3D point cloud cleaning. *IEEE/CVF International Conference on Computer Vision (ICCV)* 2019, 52–60. <https://doi.org/10.1109/ICCV.2019.00014>.
- Chaiivivatrakul, S., Tang, L., Dailey, M.N., Nakarmi, A.D., 2014. Automatic morphological trait characterization for corn plants via 3D holographic reconstruction. *Comput. Electron. Agric.* 109, 109–123. <https://doi.org/10.1016/j.compag.2014.09.005>.
- Chen, H., Wei, Z., Li, X., Xu, Y., Wei, M., Wang, J., 2022. RePCD-net: feature-Aware recurrent point cloud denoising network. *Int. J. Comput. Vis.* 130 (3), 615–629. <https://doi.org/10.1007/s11263-021-01564-7>.
- Choi, Y., Park, S., Kim, S., 2022. Development of point cloud data-denoising Technology for Earthwork Sites Using Encoder-Decoder Network. *KSCE J. Civ. Eng.* 26 (11), 4380–4389. <https://doi.org/10.1007/s12205-022-0407-8>.
- Conn, A., Pedmale, U.V., Chory, J., Navlakha, S., 2017. High-resolution laser scanning reveals plant architectures that reflect universal network design principles. *Cell Syst.* 5 (1), 53–62.e3. <https://doi.org/10.1016/j.cels.2017.06.017>.
- Das Choudhury, S., Samal, A., Awada, T., 2019. Leveraging image analysis for high-throughput plant phenotyping. *Front. Plant Sci.* 10 <https://doi.org/10.3389/fpls.2019.00508>.
- Desbrun, M., Meyer, M., Schröder, P., & Barr, A. H. (1999). Implicit fairing of irregular meshes using diffusion and curvature flow. *Proceedings of the 26th Annual Conference on Computer Graphics and Interactive Techniques*, 317–324. USA: ACM Press/Addison-Wesley Publishing Co. 10.1145/311535.311576.
- Du, R., Ma, Z., Xie, P., He, Y., Cen, H., 2023. PST: plant segmentation transformer for 3D point clouds of rapeseed plants at the podding stage. *ISPRS J. Photogramm. Remote Sens.* 195, 380–392. <https://doi.org/10.1016/j.isprsjprs.2022.11.022>.
- Fan, H., Su, H., Guibas, L., 2017. A point set generation network for 3D object reconstruction from a single image. *IEEE Conference on Computer Vision and Pattern Recognition (CVPR)* 2017, 2463–2471. <https://doi.org/10.1109/CVPR.2017.264>.
- Fan, J., Zhang, Y., Wen, W., Gu, S., Lu, X., Guo, X., 2021. The future of internet of things in agriculture: plant high-throughput phenotypic platform. *J. Clean. Prod.* 280, 123651. <https://doi.org/10.1016/j.jclepro.2020.123651>.
- Ghahremani, M., Williams, K., Corke, F., Tiddeman, B., Liu, Y., Wang, X., Doonan, J.H., 2021. Direct and accurate feature extraction from 3D point clouds of plants using RANSAC. *Comput. Electron. Agric.* 187, 106240. <https://doi.org/10.1016/j.compag.2021.106240>.
- Gu, J., Zhang, Y., Yin, Y., Wang, R., Deng, J., Zhang, B., 2022. Surface defect detection of cabbage based on curvature features of 3D point cloud. *Front. Plant Sci.* 13 <https://doi.org/10.3389/fpls.2022.942040>.
- Guerrero, P., Kleiman, Y., Ovsjanikov, M., Mitra, N.J., 2018. PCPNet Learning local shape properties from raw point clouds. *Comput. Graphics Forum* 37 (2), 75–85. <https://doi.org/10.1111/cgf.13343>.
- He, K., Zhang, X., Ren, S., Sun, J., 2016. Deep residual Learning for image recognition. *IEEE Conference on Computer Vision and Pattern Recognition (CVPR)* 2016, 770–778. <https://doi.org/10.1109/CVPR.2016.90>.
- Huang, A., Xie, Q., Wang, Z., Lu, D., Wei, M., Wang, J., 2022. MODNet: multi-offset point cloud denoising network customized for multi-scale patches. *Comput. Graphics Forum* 41 (7), 109–119. <https://doi.org/10.1111/cgf.14661>.
- Hyvärinen, A., 2005. Estimation of non-normalized statistical models by score matching. *J. Mach. Learn. Res.* 6, 695–709. <https://dl.acm.org/doi/10.5555/1046920.1088696>.
- Jiang, M., Wu, Y., Zhao, T., Zhao, Z., & Lu, C. (2018, November 23). *PointSIFT: A SIFT-like Network Module for 3D Point Cloud Semantic Segmentation*. arXiv. 10.48550/arXiv.1807.00652.
- Keller, J.M., Gray, M.R., Givens, J.A., 1985. A fuzzy K-nearest neighbor algorithm. *IEEE Trans. Syst. Man Cybern. SMC-15* (4), 580–585. <https://doi.org/10.1109/TSMC.1985.6313426>.
- Li, Z., Guo, R., Li, M., Chen, Y., Li, G., 2020. A review of computer vision technologies for plant phenotyping. *Comput. Electron. Agric.* 176, 105672. <https://doi.org/10.1016/j.compag.2020.105672>.
- Li, Z., Pan, W., Wang, S., Tang, X., Hu, H., 2023. A point cloud denoising network based on manifold in an unknown noisy environment. *Infrared Phys. Technol.* 132, 104735. <https://doi.org/10.1016/j.infrared.2023.104735>.
- Li, Y., Sheng, H., 2023. A single-stage point cloud cleaning network for outlier removal and denoising. *Pattern Recogn.* 138, 109366. <https://doi.org/10.1016/j.patcog.2023.109366>.
- Li, D., Shi, G., Li, J., Chen, Y., Zhang, S., Xiang, S., Jin, S., 2022. PlantNet: a dual-function point cloud segmentation network for multiple plant species. *ISPRS J. Photogramm. Remote Sens.* 184, 243–263. <https://doi.org/10.1016/j.isprsjprs.2022.01.007>.
- Lin, C., Hu, F., Peng, J., Wang, J., Zhai, R., 2022. Segmentation and stratification methods of field maize terrestrial LiDAR point cloud. *Agriculture* 12 (9), 1450. <https://doi.org/10.3390/agriculture12091450>.
- Liu, Y., Yuan, H., Zhao, X., Fan, C., Cheng, M., 2023. Fast reconstruction method of three-dimension model based on dual RGB-D cameras for peanut plant. *Plant Methods* 19 (1), 17. <https://doi.org/10.1186/s13007-023-0098-z>.
- Lu, X., Ono, E., Lu, S., Zhang, Y., Teng, P., Aono, M., Omasa, K., 2020. Reconstruction method and optimum range of camera-shooting angle for 3D plant modeling using a multi-camera photography system. *Plant Methods* 16 (1), 118. <https://doi.org/10.1186/s13007-020-00658-6>.
- Luo, S., & Hu, W. (2020). Differentiable Manifold Reconstruction for Point Cloud Denoising. *Proceedings of the 28th ACM International Conference on Multimedia*, 1330–1338. New York, NY, USA: Association for Computing Machinery. 10.1145/3394171.3413727.
- Luo, S., Hu, W., 2021. Score-based point cloud denoising. *IEEE/CVF International Conference on Computer Vision (ICCV)* 2021, 4563–4572. <https://doi.org/10.1109/ICCV48922.2021.00454>.
- Miao, Y., Peng, C., Wang, L., Qiu, R., Li, H., Zhang, M., 2022. Measurement method of maize morphological parameters based on point cloud image conversion. *Comput. Electron. Agric.* 199, 107174. <https://doi.org/10.1016/j.compag.2022.107174>.
- Miao, T., Zhu, C., Xu, T., Yang, T., Li, N., Zhou, Y., Deng, H., 2021. Automatic stem-leaf segmentation of maize shoots using three-dimensional point cloud. *Comput. Electron. Agric.* 187, 106310. <https://doi.org/10.1016/j.compag.2021.106310>.
- Paturkar, A., Sen Gupta, G., Bailey, D., 2021. Making use of 3D models for plant physiognomic analysis: a review. *Remote Sens. (Basel)* 13 (11), 2232. <https://doi.org/10.3390/rs13112232>.
- Pistilli, F., Fracastoro, G., Valsesia, D., & Magli, E. (2020). Learning Graph-Convolutional Representations for Point Cloud Denoising. In A. Vedaldi, H. Bischof, T. Brox, & J.-M. Frahm (Eds.), *Computer Vision – ECCV 2020* (pp. 103–118). Cham: Springer International Publishing. 10.1007/978-3-030-58565-5_7.
- Qi, C. R., Yi, L., Su, H., & Guibas, L. J. (2017). PointNet++: Deep Hierarchical Feature Learning on Point Sets in a Metric Space. *Advances in Neural Information Processing Systems* 30, 5099–5108. Long Beach: Curran Associates, Inc.
- Qi, C.R., Su, H., Mo, K., Guibas, L.J., 2017a. PointNet deep Learning on point sets for 3D classification and segmentation. *IEEE Conference on Computer Vision and Pattern Recognition (CVPR)* 2017, 77–85. <https://doi.org/10.1109/CVPR.2017.16>.
- Rakotosaona, M.-J., La Barbera, V., Guerrero, P., Mitra, N.J., Ovsjanikov, M., 2020. PointCleanNet: Learning to denoise and remove outliers from dense point clouds. *Comput. Graphics Forum* 39 (1), 185–203. <https://doi.org/10.1111/cgf.13753>.
- Rusu, R.B., Cousins, S., 2011. 3D is here: point cloud Library (PCL). *IEEE Int. Conf. Robot. Autom.* 2011, 1–4. <https://doi.org/10.1109/ICRA.2011.5980567>.
- Schunck, D., Magistri, F., Rosu, R.A., Cornelissen, A., Chebrolu, N., Paulus, S., Klingbeil, L., 2021. Pheno4D: a spatio-temporal dataset of maize and tomato plant point clouds for phenotyping and advanced plant analysis. *PLoS One* 16 (8), e0256340.

- Song, P., Li, Z., Yang, M., Shao, Y., Pu, Z., Yang, W., Zhai, R., 2023. Dynamic detection of three-dimensional crop phenotypes based on a consumer-grade RGB-D camera. *Front. Plant Sci.* 14 <https://doi.org/10.3389/fpls.2023.109725>.
- Turgut, K., Dutagaci, H., Galopin, G., Rousseau, D., 2022a. Segmentation of structural parts of rosebush plants with 3D point-based deep learning methods. *Plant Methods* 18 (1), 20. <https://doi.org/10.1186/s13007-022-00857-3>.
- Turgut, K., Dutagaci, H., Rousseau, D., 2022b. RoseSegNet: an attention-based deep learning architecture for organ segmentation of plants. *Biosyst. Eng.* 221, 138–153. <https://doi.org/10.1016/j.biosystemseng.2022.06.016>.
- Wang, Z., Sun, W., & Tian, L. (2023). 3D Point Cloud Denoising Based on Hybrid Attention Mechanism and Score Matching. *Proceedings of the 2022 5th International Conference on Artificial Intelligence and Pattern Recognition*, 767–772. New York, NY, USA: Association for Computing Machinery. 10.1145/3573942.3574093.
- Wang, Y., Sun, Y., Liu, Z., Sarma, S.E., Bronstein, M.M., Solomon, J.M., 2019. Dynamic graph CNN for Learning on point clouds. *ACM Trans. Graph.* 38 (5), 146:1–146:12. <https://doi.org/10.1145/3326362>.
- Wei, B., Ma, X., Guan, H., Yu, M., Yang, C., He, H., Shen, P., 2023. Dynamic simulation of leaf area index for the soybean canopy based on 3D reconstruction. *Eco. Inform.* 75, 102070 <https://doi.org/10.1016/j.ecoinf.2023.102070>.
- White, J.W., Andrade-Sanchez, P., Gore, M.A., Bronson, K.F., Coffelt, T.A., Conley, M.M., Wang, G., 2012. Field-based phenomics for plant genetics research. *Field Crop Res* 133, 101–112. <https://doi.org/10.1016/j.fcr.2012.04.003>.
- Wu, S., Wen, W., Wang, Y., Fan, J., Wang, C., Gou, W., & Guo, X. (2020). MVS-Pheno: A Portable and Low-Cost Phenotyping Platform for Maize Shoots Using Multiview Stereo 3D Reconstruction. *Plant Phenomics* (2020), 2020/1848437. 10.34133/2020/1848437.
- Wu, S., Wen, W., Xiao, B., Guo, X., Du, J., Wang, C., Wang, Y., 2019. An accurate skeleton Extraction approach from 3D point clouds of maize plants. *Front. Plant Sci.* 10 <https://doi.org/10.3389/fpls.2019.00248>.
- Wu, J., Xue, X., Zhang, S., Qin, W., Chen, C., Sun, T., 2018. Plant 3D reconstruction based on LiDAR and multi-view sequence images. *Int. J. Precis. Agric. Aviat.* 1 (1) <https://doi.org/10.33440/j.ijpaa.20180101.0007>.
- Xiang, L., Nolan, T.M., Bao, Y., Elmore, M., Tuel, T., Gai, J., Tang, L., 2021. Robotic assay for drought (RoAD): an automated phenotyping system for brassinosteroid and drought responses. *Plant J.* 107 (6), 1837–1853. <https://doi.org/10.1111/TPJ.15401>.
- Xu, X., Geng, G., Cao, X., Li, K., Zhou, M., 2022. TDNet: Transformer-based network for point cloud denoising. *Appl. Opt.* 61 (6), C80–C88. <https://doi.org/10.1364/AO.438396>.
- Yamamoto, S., Karkee, M., Kobayashi, Y., Nakayama, N., Tsubota, S., Thi Thanh, L.N., Konya, T., 2018. 3D reconstruction of apple fruits using consumer-grade RGB-depth sensor. *Eng. Agric. Environ. Food* 11 (4), 159–168. <https://doi.org/10.1016/j.eaef.2018.02.005>.
- Yau, W.K., Ng, O.-E., Lee, S.W., 2021. Portable device for contactless, non-destructive and in situ outdoor individual leaf area measurement. *Comput. Electron. Agric.* 187, 106278 <https://doi.org/10.1016/j.compag.2021.106278>.
- Zermas, D., Morellas, V., Mulla, D., Papanikolopoulos, N., 2020. 3D model processing for high throughput phenotype extraction – the case of corn. *Comput. Electron. Agric.* 172, 105047 <https://doi.org/10.1016/j.compag.2019.105047>.
- Zhang, D., Lu, X., Qin, H., He, Y., 2021. Pointfilter: point cloud filtering via encoder-decoder modeling. *IEEE Trans. Vis. Comput. Graph.* 27 (3), 2015–2027. <https://doi.org/10.1109/TVCG.2020.3027069>.
- Zhao, T., Gao, P., Tian, T., Ma, J., Tian, J., 2022. From noise addition to denoising: a self-Variation capture network for point cloud optimization. *IEEE Trans. Vis. Comput. Graph.* 1–14 <https://doi.org/10.1109/TVCG.2022.3231680>.
- Zhao, Y., Zheng, H., Wang, Z., Luo, J., Lam, E.Y., 2023. Point cloud denoising via momentum ascent in gradient fields. *IEEE International Conference on Image Processing (ICIP) 2023*, 161–165. <https://doi.org/10.1109/ICIP49359.2023.10222122>.
- Zhu, T., Ma, X., Guan, H., Wu, X., Wang, F., Yang, C., Jiang, Q., 2023b. A calculation method of phenotypic traits based on three-dimensional reconstruction of tomato canopy. *Comput. Electron. Agric.* 204, 107515 <https://doi.org/10.1016/j.compag.2022.107515>.
- Zhu, B., Zhang, Y., Sun, Y., Shi, Y., Ma, Y., Guo, Y., 2023a. Quantitative estimation of organ-scale phenotypic parameters of field crops through 3D modeling using extremely low altitude UAV images. *Comput. Electron. Agric.* 210, 107910 <https://doi.org/10.1016/j.compag.2023.107910>.
- Zhao, C., Zhang, Y., Du, J., Guo, X., Wen, W., Gu, S., Fan, J., 2019. Crop Phenomics: Current Status and Perspectives. *Front. Plant Sci.* 10 <https://doi.org/10.3389/fpls.2019.00714>.